

## Article

# Primary Minerals and Age of The Hydrothermal Quartz Veins Containing U-Mo-(Pb, Bi, Te) Mineralization in the Majerská Valley near Čučma (Gemic Unit, Spišsko-Gemerské Rudohorie Mts., Slovak Republic)

Štefan Ferenc <sup>1,\*</sup>, Martin Šteško <sup>2,3</sup> , Tomáš Mikuš <sup>4</sup>, Stanislava Milovská <sup>4</sup>, Richard Kopáček <sup>1</sup> and Eva Hoppanová <sup>1</sup>

<sup>1</sup> Department of Geography and Geology, Faculty of Natural Sciences, Matej Bel University, Tajovského 40, 974 01 Banská Bystrica, Slovakia; richard.kopacik@umb.sk (R.K.); eva.hoppanova@umb.sk (E.H.)

<sup>2</sup> Earth Science Institute of the Slovak Academy of Sciences, Dúbravská cesta 9, 840 05 Bratislava, Slovakia; msminerals@gmail.com

<sup>3</sup> Department of Mineralogy and Petrology, National Museum, Cirkusová 1740, 193 00 Praha 9, Horní Počernice, Czech Republic

<sup>4</sup> Earth Science Institute of the Slovak Academy of Sciences, Ďumbierska 1, 974 11 Banská Bystrica, Slovakia; mikus@savbb.sk (T.M.); milovska@savbb.sk (S.M.)

\* Correspondence: stefan.ferenc@umb.sk; Tel.: +421-048-446-7253



**Citation:** Ferenc, Š.; Šteško, M.; Mikuš, T.; Milovská, S.; Kopáček, R.; Hoppanová, E. Primary Minerals and Age of The Hydrothermal Quartz Veins Containing U-Mo-(Pb, Bi, Te) Mineralization in the Majerská Valley near Čučma (Gemic Unit, Spišsko-Gemerské Rudohorie Mts., Slovak Republic). *Minerals* **2021**, *11*, 629. <https://doi.org/10.3390/min11060629>

Academic Editors: Jaroslav Pršek and Jiří Sejkora

Received: 7 May 2021

Accepted: 10 June 2021

Published: 13 June 2021

**Publisher's Note:** MDPI stays neutral with regard to jurisdictional claims in published maps and institutional affiliations.



**Copyright:** © 2021 by the authors. Licensee MDPI, Basel, Switzerland. This article is an open access article distributed under the terms and conditions of the Creative Commons Attribution (CC BY) license (<https://creativecommons.org/licenses/by/4.0/>).

**Abstract:** An occurrence of vein U-Mo mineralization is located in the Majerská valley near Čučma, about 7 km to the NNE of the district town of Rožňava (Eastern Slovakia). Mineralization is hosted in the acidic metapyroclastics of the Silurian Bystrý Potok Fm. (Gemic Unit), and originated in the following stages: (I.) quartz I, fluorapatite I; (II.) quartz II, fluorapatite II, zircon, rutile chlorite, tourmaline; (III.) uraninite, molybdenite, U-Ti oxides; (IV.) pyrite I, ullmannite, gersdorffite, cobaltite; (Va.) galena, bismuth, tetradymite, joséite A and B, Bi<sub>3</sub>(TeS)<sub>2</sub> mineral phase, (BiPb)(TeS) mineral phase, ikonolite; (Vb.) minerals of the kobellite–tintinaite series, cosalite; (VI.) pyrite II; (VII.) titanite, chlorite; and (VIII.) supergene mineral phases. The chemical in-situ electron-microprobe U-Pb dating of uraninite from a studied vein yielded an average age of around 265 Ma, corresponding to the Guadalupian Epoch of Permian; the obtained data corresponds with the age of Gemic S-type granites. The age correlation of uraninite with the Gemic S-type granites and the spatial connection of the studied mineralization with the Čučma granite allows us to assume that it is a Hercynian, granite-related (perigranitic) mineralization.

**Keywords:** uranium; vein mineralization; uraninite; molybdenite; sulphotellurides; uraninite dating; Permian; Gemic Unit; Gemic granites; Western Carpathians

## 1. Introduction

Radioactive anomalies in the vicinity of the Čučma village, north of the district town Rožňava (Eastern Slovakia), were, in the past, a subject of several repeated geological surveys or mineralogical-geochemical research [1–13]. These works were focused on the prospecting, possible verification of raw materials resources and more detailed genetic or mineralogical-geochemical study of U, REE and Au ores. Unfortunately, the results of the geological survey did not show their economic significance.

The above-mentioned anomalies are related to the hydrothermal quartz (quartz-apatite respectively) veins with U mineralization, which are hosted mainly in metarhyolites and their metapyroclastics, less in graphite-sericite, graphite and chlorite-rich phyllites (Lower Paleozoic, Gelnica Group, Gemic Unit). The veins are located in the proximity (a maximum of several hundred meters) of the Permian Gemic granites intrusions.

In the area of the Majerská valley near Čučma, the following two types of these veins can be distinguished, based on their mineral composition:

(A) Quartz-fluorapatite veins containing xenotime-(Y), monazite-(Ce) monazite-(Nd), allanite-(Ce), pyrite, marcasite, uraninite, brannerite, rutile, muscovite, dravite and titanite (primary minerals); goethite, plumbogummite, goyazite, florencite-(Ce), autunite and torbernite (supergene minerals). The mentioned minerals are accompanied by younger (Alpine?) mineral associations represented by quartz II, siderite, dolomite, pyrite, arsenopyrite, pyrrhotite, marcasite, tetrahedrite, chalcopyrite, sphalerite, jamesonite, etc.

(B) Quartz veins, with only accessory amount of fluorapatite and zircon, titanite, muscovite, chlorites, rutile, leucogenized Fe-Ti oxides and rarely U-Ti oxides. Ore mineralization is represented mainly by abundant uraninite and molybdenite. Supergene minerals are represented by bassetite, saléeite, autunite, torbernite, zeunerite, phosphuranylite, iriginite, U-rich wulfenite and other, poorly identified Pb-Bi-U-Mo minerals.

The presented contribution is devoted to the results of the detailed mineralogical research of primary minerals association, and CHIME dating of uraninite, from the quartz veins with U-Mo mineralization (the above-mentioned B type), which, thus far, has been insufficiently investigated. These veins are characterized by a unique mineral association, and the mineral phases often have an unusual chemical composition or are rare also on a global scale. In addition, CHIME dating of uraninite clarifies the genetic relationship of the vein U mineralization in the Gemic Unit to the Permian S-type granite magmatism and brings new insights into the issue of the Western Carpathians metallogeny.

## 2. Regional Geological Setting

The Gemic Unit is one of the most important tectonic superunits in the Western Carpathians. In the north, it is thrust along the Čertovica tectonic line over the Tatric Unit; in the south, the Gemic Unit is limited by the Lubeník–Margecany tectonic line, which separates it from the overlying Veporic Unit (Figure 1A). The Gemic Unit forms a system of north-vergent partial nappes that are composed mainly of metamorphic pre-Carboniferous complexes and Late Paleozoic (to- Lower Triassic) syn- and post-orogenic formations [14]. It is most often divided into a northern (Klátov, Rakovec, Črmeľ and Ochtiná Units) and a southern (Gelnica Group and Štós Unit) part. The Gelnica Group is represented by several thousand meters of thick Paleozoic volcanogenic (rhyolite–dacite) flysch [15,16], and its origin was associated with an active margin of Gondwana [17,18]. Both sedimentary and volcanic rocks have undergone regional metamorphism under the chlorite zone of the greenschist-facies conditions [19,20]. The Gelnica Group is, from the bottom to top, divided into the Vlachovo, Bystrý Potok and Drnava Formations (sensu [16,21,22]) intruded by the Permian S-type Gemic granites [23]. According to geophysics data, these are apophyses of a larger granite body underlying metamorphosed volcano-sedimentary sequences of the Gemic Unit [24].

All three of the following formations (sensu [16,21]) of the Gelnica Group: the Vlachovo Fm. (Lower–Middle Silurian), the Bystrý Potok Fm. (Middle Silurian) and the Lower Devonian Drnava Fm. (Figure 1B) are present within the studied area. The Bystrý potok Fm. is the most widespread, formed mainly by lydites, quartz-sericite or graphitic phyllites, metamorphosed rhyolites, dacites and their pyroclastics. Although, according to published geological maps, the Bystrý Potok Fm. is stratigraphically assigned to the Silurian [16], its magmatic rocks yielded Middle–Late Ordovician U–Th–Pb SHRIMP zircon ages of  $465.8 \pm 1.5$  Ma [18,25] and 460–465 Ma, respectively [26]. According to a concept by Grecula et al. [27,28], rhyolite metapyroclastics rocks (so-called porphyroids) of the Bystrý Potok Fm. are included in the Smolník Fm., and metasediments presented as eyed to gneissed metapelites, quartzites or quartzite gneisses represent the Betliar Fm. The Drnava Fm. formed by quartz, chlorite-sericite, or graphitic-sericite phyllites with acidic metapyroclastic rocks is defined by Grecula et al. [27,28] as the Betliar Fm. The metacarbonates of the Vlachovo Fm. are also considered as part of the Betliar Fm. These authors present

the stratigraphic range of both the Smolník and the Betliar Formations as Ordovician to Devonian.

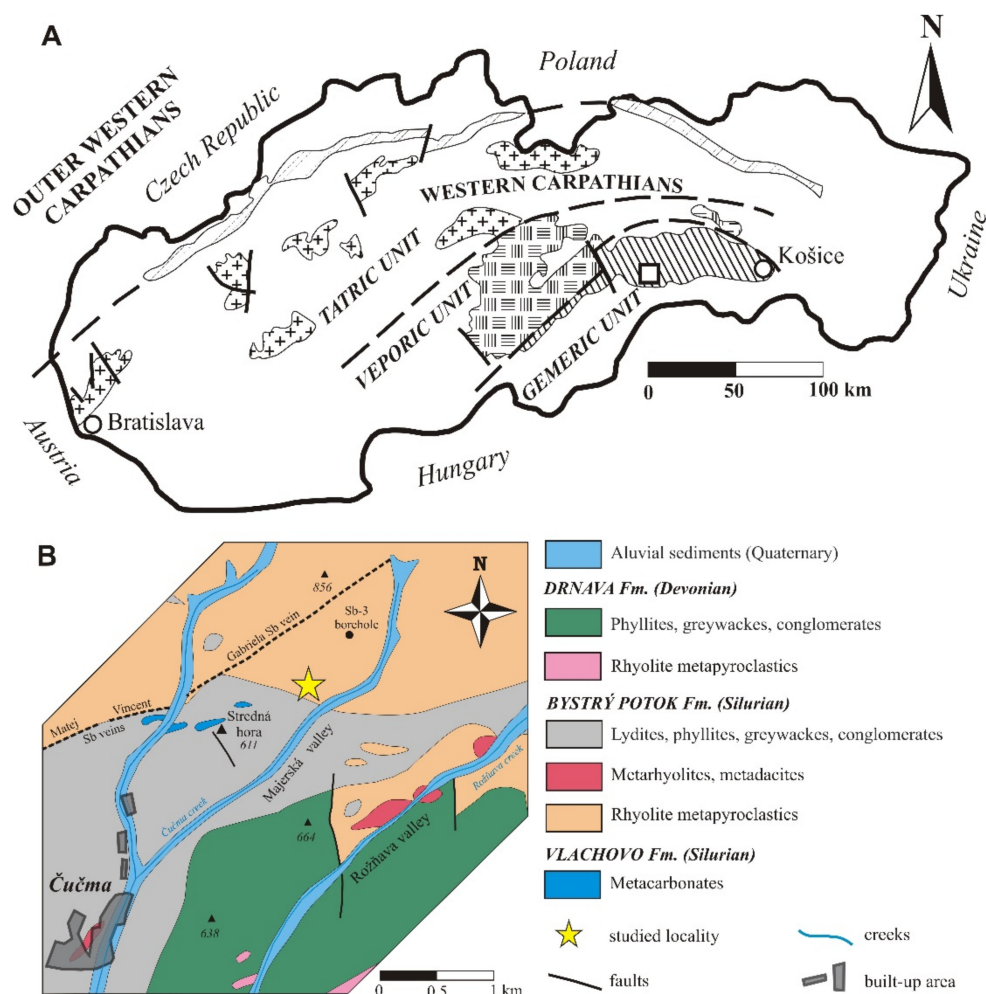


**Figure 1.** (A) Position of the studied locality (white square) within the main Alpine tectonic units of the Western Carpathians; (B) Geological map of the surroundings of the vein U-Mo mineralization occurrence near Čučma. According to [22].

#### Localization and Geology of The Studied Occurrence

The occurrence of the vein U-Mo mineralization is located in the Majerská valley near Čučma. The site is located about 7 km to the NNE of the district town Rožňava, 3.5 km to the NE of the center of the Čučma village, 950 m to the S of the elevation of 856 m (Lázpatak), at an altitude of about 580–630 m. The geographical coordinates of the occurrence are E 20.568018° and N 48.714321°.

The studied vein with U-Mo mineralization is hosted in the acidic metapyroclastics (porphyroids) of the Silurian Bystrý Potok Fm. (Figure 1B). Three veins, arranged in accordance with the metamorphic foliation of the surrounding rocks, were discovered in the area of the Majerská valley occurrence in the 1960s. The veins have a direction of 65–67° to the NE, with a dip of about 36° to the SE. They are 0.1 to 0.3 m thick and reach a length of up to 50 m. The veins have a lenticular character, to thin out rapidly along strike and dip [1]. The mineralogy of the primary minerals of this occurrence has not yet been studied in more detail. Only quartz, apatite, uraninite and pyrite have been described within the primary vein filling [1].

### 3. Methods Used

Field samples were collected using an SGR scintillation radiometer (sample activity measured in cps), at a measuring range (sensitivity) of 400–3000 keV and a measurement step of 0.2 s. Uncovered polished sections were then made from the samples for microscopic study in both transmitted and reflected light.

In situ CHIME dating of uraninite [29] was performed on a Cameca SX100 electron microanalyzer at the Dionýz Štúr State Geological Institute in Bratislava (analyzed by P. Konečný). The following conditions were used for the measurement: accelerating voltage, 15 kV; measuring current, 80–150 nA; measuring time, 75–130 s; electron beam diameter, 1–5  $\mu\text{m}$ . The used standards and spectral lines are as follows:  $\text{UO}_2$  ( $\text{UM}\beta$ ),  $\text{Al}_2\text{O}_3$  ( $\text{AlK}\alpha$ ), wollastonite ( $\text{CaK}\alpha$ ,  $\text{SiK}\alpha$ ), GaAs ( $\text{AsL}\alpha$ ), apatite ( $\text{PK}\alpha$ ),  $\text{PbCO}_3$  ( $\text{PbM}\alpha$ ),  $\text{ThO}_2$  ( $\text{ThM}\alpha$ ), baryte ( $\text{SK}\alpha$ ),  $\text{SrTiO}_3$  ( $\text{SrL}\alpha$ ), fayalite ( $\text{FeK}\alpha$ ),  $\text{YPO}_4$  ( $\text{YL}\alpha$ ),  $\text{LaPO}_4$  ( $\text{LaL}\alpha$ ),  $\text{CePO}_4$  ( $\text{CeL}\alpha$ ),  $\text{PrPO}_4$  ( $\text{PrL}\beta$ ),  $\text{NdPO}_4$  ( $\text{NdL}\alpha$ ),  $\text{SmPO}_4$  ( $\text{SmL}\alpha$ ),  $\text{EuPO}_4$  ( $\text{EuL}\beta$ ),  $\text{GdPO}_4$  ( $\text{GdL}\alpha$ ),  $\text{TbPO}_4$  ( $\text{TbL}\alpha$ ),  $\text{DyPO}_4$  ( $\text{DyL}\beta$ ),  $\text{HoPO}_4$  ( $\text{HoL}\beta$ ),  $\text{ErPO}_4$  ( $\text{ErL}\beta$ ),  $\text{TmPO}_4$  ( $\text{TmL}\alpha$ ),  $\text{YbPO}_4$  ( $\text{YbL}\alpha$ ) and  $\text{LuPO}_4$  ( $\text{LuL}\beta$ ). The detection limit for the individual elements ranged from 0.01–0.1 wt. %. Elements with content below the detection limit are not included in the tables. The following corrections were used for interferences, especially in the case of rare earth elements:  $\text{Pb} \times \text{Y}$ , 0.008029;  $\text{U} \times \text{Th}$ , 0.00704;  $\text{Gd} \times \text{La}$ , 0.017352;  $\text{Gd} \times \text{Ce}$ , 0.073999;  $\text{Er} \times \text{Gd}$ , 0.027983;  $\text{Lu} \times \text{Yb}$ , 0.03688;  $\text{Lu} \times \text{Dy}$ , 0.051522;  $\text{Ho} \times \text{Gd}$ , 0.017001;  $\text{Lu} \times \text{Ho}$ , 0.068289;  $\text{Eu} \times \text{Dy}$ , 0.12;  $\text{Er} \times \text{Eu}$ , 0.022131; and  $\text{Tm} \times \text{Sm}$ , 0.11517.

The chemical composition of other minerals was determined using an Jeol-JXA-8530F electron microprobe (Institute of Earth Sciences SAS, Banská Bystrica). A microanalyzer was used for a quick determination of the chemical composition of minerals by means of an energy-dispersive spectrum (EDS), as well as for point wave dispersion microanalysis (WDS). WDS microanalyses were performed under the following conditions: accelerating voltage, 15 kV; measuring current, 20 nA (apatite) and 20 kV; measuring current, 15 nA (sulphides and sulphosalts). The diameter of the electron beam was in the range of 2–8  $\mu\text{m}$ , and ZAF correction was used. The natural/synthetic standards used and their spectral lines were as follows: Ag ( $\text{L}\alpha$ )—Ag, Sb ( $\text{L}\alpha$ )—stibnite, Hg ( $\text{M}\alpha$ )—cinnabar, Ni ( $\text{K}\alpha$ )—gersdorffite, Zn ( $\text{K}\alpha$ )—sphalerite, Cd ( $\text{L}\alpha$ )—CdTe, Au ( $\text{M}\alpha$ )—Au, Ca ( $\text{K}\alpha$ )—diopside, K ( $\text{K}\alpha$ )—orthoclase, U ( $\text{M}\beta$ )— $\text{UO}_2$ , Th ( $\text{M}\alpha$ )—thorianite, Pb ( $\text{M}\beta$ )—crocoite, S ( $\text{K}\alpha$ )—baryte, P ( $\text{K}\alpha$ )—apatite, Y ( $\text{L}\alpha$ )— $\text{YPO}_4$ , Hf ( $\text{M}\alpha$ )— $\text{ZrO}_2(\text{kub.})$ , Zr ( $\text{L}\beta$ )— $\text{ZrO}_2(\text{kub.})$ , F ( $\text{K}\alpha$ )—fluorite, Cl ( $\text{K}\alpha$ )—tugtupite, Na ( $\text{K}\alpha$ )—albite, Sr ( $\text{L}\alpha$ )—celestite, Si ( $\text{K}\alpha$ )—orthoclase, Al ( $\text{K}\alpha$ )—albite, As ( $\text{L}\alpha$ )—GaAs, Mg ( $\text{K}\alpha$ )—diopside, Lu ( $\text{L}\alpha$ )— $\text{LuPO}_4$ , Ho ( $\text{L}\beta$ )— $\text{HoPO}_4$ , Yb ( $\text{L}\alpha$ )— $\text{YbPO}_4$ , Tm ( $\text{L}\alpha$ )— $\text{TmPO}_4$ , Er ( $\text{L}\alpha$ )— $\text{ErPO}_4$ , Gd ( $\text{L}\beta$ )— $\text{GdPO}_4$ , Dy ( $\text{L}\alpha$ )— $\text{DyPO}_4$ , Tb ( $\text{L}\alpha$ )— $\text{TbPO}_4$ , Sm ( $\text{L}\beta$ )— $\text{SmPO}_4$ , Eu ( $\text{L}\alpha$ )— $\text{EuPO}_4$ , Pr ( $\text{L}\beta$ )— $\text{PrPO}_4$ , Nd ( $\text{L}\alpha$ )— $\text{NdPO}_4$ , Ce ( $\text{L}\alpha$ )— $\text{CePO}_4$ , La ( $\text{L}\alpha$ )— $\text{LaPO}_4$ , Co ( $\text{K}\alpha$ )—Co, Zn ( $\text{K}\alpha$ )—gahnite, Cu ( $\text{K}\alpha$ )—cuprite, Fe ( $\text{K}\alpha$ )—olivine, Mn ( $\text{K}\alpha$ )—rhodonite, Ti ( $\text{K}\alpha$ )—rutile, Ba ( $\text{L}\alpha$ )—baryte, Te ( $\text{L}\alpha$ )—CdTe, Se ( $\text{L}\beta$ )— $\text{Bi}_2\text{Se}_3$ , Sn ( $\text{L}\alpha$ )— $\text{SnO}_2$ , W ( $\text{M}\alpha$ )— $\text{CaWO}_4$ , Mo ( $\text{L}\alpha$ )—wulfenite, Cr ( $\text{K}\alpha$ )— $\text{Cr}_2\text{O}_3$ , Bi ( $\text{M}\alpha$ )— $\text{Bi}_2\text{Se}_3$ .

Part of quantitative chemical analyses of ore minerals were performed also on a Cameca SX100 electron-microprobe (Department of Mineralogy and Petrology, National Museum, Prague, Czech Republic), operating in the wavelength-dispersive (WDS) mode (25 kV, 20 nA and 2 to 5  $\mu\text{m}$  wide beam). The following standards and X-ray lines were used (DL—detection limit): Ag ( $\text{AgL}\alpha$  DL 0.07), Bi ( $\text{BiM}\beta$  DL 0.28), CdTe ( $\text{CdL}\alpha$  DL 0.07), chalcopyrite ( $\text{CuK}\alpha$  DL 0.05,  $\text{SK}\alpha$  DL 0.05), Co ( $\text{CoK}\alpha$  DL 0.04), halite ( $\text{ClK}\alpha$  DL 0.04), HgTe ( $\text{HgL}\alpha$  DL 0.27), InAs ( $\text{InL}\alpha$  DL 0.05), Mn ( $\text{MnK}\alpha$  DL 0.04), Ni ( $\text{NiK}\alpha$  DL 0.04), NiAs ( $\text{AsL}\alpha$  DL 0.06), PbS ( $\text{PbM}\alpha$  DL 0.11), PbSe ( $\text{SeL}\beta$  DL 0.08), pyrite ( $\text{FeK}\alpha$  DL 0.04), Sb<sub>2</sub>S<sub>3</sub> ( $\text{SbL}\alpha$  DL 0.05), Sn ( $\text{SnL}\alpha$  DL 0.05), PbTe ( $\text{TeL}\alpha$  DL 0.06) and ZnS ( $\text{ZnK}\alpha$  DL 0.06). The contents of the above-listed elements, which are not included in the tables, were analyzed quantitatively, but their contents were below the detection limit. Raw intensities were converted to the concentrations of elements using automatic “PAP” matrix-correction software [30].

The distribution maps of the individual elements in a typical ore material were made using X-ray fluorescence spectroscopy (XRF) at the Institute of Earth Sciences SAS in Banská

Bystrica, using an M4 TORNADO instrument (Bruker) under the following conditions: current, 50 kV; voltage, 600  $\mu$ A; range, 40 keV/130 kcps; and measurement time, 2 h.

Chemical analyses of the mineralized samples were performed using the Inductively Coupled Plasma-Emission Spectrometry (ICP-ES) and Inductively Coupled Plasma-Mass Spectrometry (ICP-MS) analyses (ACME Analytical Laboratories Ltd., Vancouver, BC, Canada).

## 4. Results

### 4.1. Character of Mineralization

Quartz is a dominant gangue mineral. It has a white to grey-white color locally with a slight pinkish tint. Quartz gangue is relatively compact, and small drusy cavities are rare. Accessory minerals are represented by fluorapatite, zircon, titanite, muscovite, chlorites, tourmaline (schorl to dravite), rutile, leucoxenized Fe-Ti oxides and, rarely, U-Ti oxides. U-Mo mineralization (represented mainly by uraninite and molybdenite) is distributed very irregularly. Macroscopically, it forms dark smudgy accumulations, or irregular fine-grained bands or veinlets in the quartz (up to 5–6 cm in size, Figure 2). Quartz is weakly limonitized in the vicinity of accumulations of U-Mo minerals. The radioactivity of individual collected samples is reaching up to 600–700 cps. U-Mo mineralization is often accompanied by younger, sulphidic mineralization (pyrite, sulphotellurides, sulphosalts, etc.). The chemical composition of the average mineralized gangue is illustrated in Table 1. The distribution of the individual major elements in the vein is shown in Figure 3.



**Figure 2.** Irregular veinlets of U-Mo mineralization in limonitized quartz. The small cavities in the quartz are filled with a yellow uranyl molybdate—iriginite. Photo: Š. Ferenc.

**Table 1.** Chemical composition of a quartz vein containing U-Mo mineralization (Q-U-Mo) in comparison to the composition of quartz-fluorapatite veins containing U-REE mineralization (Q-Ap-U-REE) from the Majerská Valley. Elements with significantly different content in both types of veins are highlighted in bold.

	Q-Ap-U-REE	Q-U-Mo		Q-Ap-U-REE	Q-U-Mo	
Li	2.3	3.7	ppm	In	0.03	<0.01 ppm
Na	0.032	0.016	wt. %	Tl	<0.05	0.26 ppm
K	0.2	0.19	wt. %	<b>P</b>	<b>3.039</b>	<b>0.031</b> wt. %
Rb	10.3	13.3	ppm	<b>As</b>	<b>19.9</b>	<b>1823.9</b> ppm
Cs	0.2	1.2	ppm	Sb	15.8	20.26 ppm
Be	<1	1	ppm	Bi	6.92	3.85 ppm
Mg	0.05	0.1	wt. %	Al	0.56	0.47 wt. %
<b>Ca</b>	<b>7.26</b>	<b>0.08</b>	wt. %	S	<0.04	0.08 wt. %
<b>Sr</b>	<b>204</b>	<b>16</b>	ppm	Se	<0.3	<0.3 ppm
Ba	73	39	ppm	Te	0.29	0.1 ppm
Ti	0.025	0.011	wt. %	Sc	13.7	5 ppm
Zr	0.3	1.9	ppm	<b>Y</b>	<b>104.1</b>	<b>24.5</b> ppm
Hf	<0.02	<0.02	ppm	<b>La</b>	<b>106.5</b>	<b>3.3</b> ppm
V	<1	<1	ppm	<b>Ce</b>	<b>281.8</b>	<b>8.7</b> ppm
Nb	4.25	2.37	ppm	<b>Pr</b>	<b>41.8</b>	<b>1.6</b> ppm
Ta	<0.01	<0.01	ppm	<b>Nd</b>	<b>209.5</b>	<b>9.6</b> ppm
Cr	2	2	ppm	<b>Sm</b>	<b>75.1</b>	<b>6.8</b> ppm
<b>Mo</b>	<b>1.51</b>	<b>73.36</b>	ppm	<b>Eu</b>	<b>29.2</b>	<b>1.5</b> ppm
W	37	45.1	ppm	<b>Gd</b>	<b>68.7</b>	<b>8.1</b> ppm
Sn	3.4	0.3	ppm	<b>Tb</b>	<b>10.1</b>	<b>1.7</b> ppm
Re	<0.002	<0.002	ppm	<b>Dy</b>	<b>48.5</b>	<b>10.4</b> ppm
Mn	75	23	ppm	Ho	5.7	1.4 ppm
Fe	0.3	0.45	wt. %	Er	15.4	3.7 ppm
<b>Co</b>	<b>0.4</b>	<b>7.9</b>	ppm	Tm	1.8	0.5 ppm
<b>Ni</b>	<b>0.1</b>	<b>6.3</b>	ppm	<b>Yb</b>	<b>13</b>	<b>3.6</b> ppm
Cu	41.8	37.1	ppm	Lu	1.2	0.3 ppm
Zn	3.4	9.6	ppm	Th	2.6	0.3 ppm
<b>Pb</b>	<b>189.93</b>	<b>93.23</b>	<b>ppm</b>	<b>U</b>	<b>&gt;4000</b>	<b>2639.1</b> ppm
Cd	0.03	0.17	ppm	YREE	1012.4	85.7 ppm
Ag	154	139	ppm	LREE	812.6	39.6 ppm
Ga	3.73	1.55	ppm	HREE	95.7	21.6 ppm

## 4.2. Primary Vein Minerals

### 4.2.1. Ore (Opaque) Minerals

**Molybdenite** always appears in close spatial association with uraninite, over which it usually predominates. It forms rich accumulations up to several cm in size, which consist of individual flaky crystals up to 20  $\mu\text{m}$  long (Figure 4a). Molybdenite forms rims on uraninite aggregates, respectively enclosing them (Figure 4b). The spaces between the individual molybdenite crystals are locally filled with aggregates of supergene wulfenite (Figure 4c). The chemical composition of the molybdenite from Čučma is close to the ideal formula. Only a slightly increased content of Fe (up to 0.11 wt. %; 0.003 *apfu*) was determined using WDS analysis.

**Uraninite** is the second most widespread ore mineral after molybdenite. It forms globular aggregates up to 0.1 mm in size (the average size of globules is about 30–40  $\mu\text{m}$ ) and their clusters (also irregular aggregates), in direct association with molybdenite (Figure 4a–c). Locally, it also forms grains enclosed in fluorapatite. The supergene degradation of uraninite is manifested by the formation of uranyl phosphates, especially saléeite and bassetite in the close vicinity of its aggregates (Figure 4d).

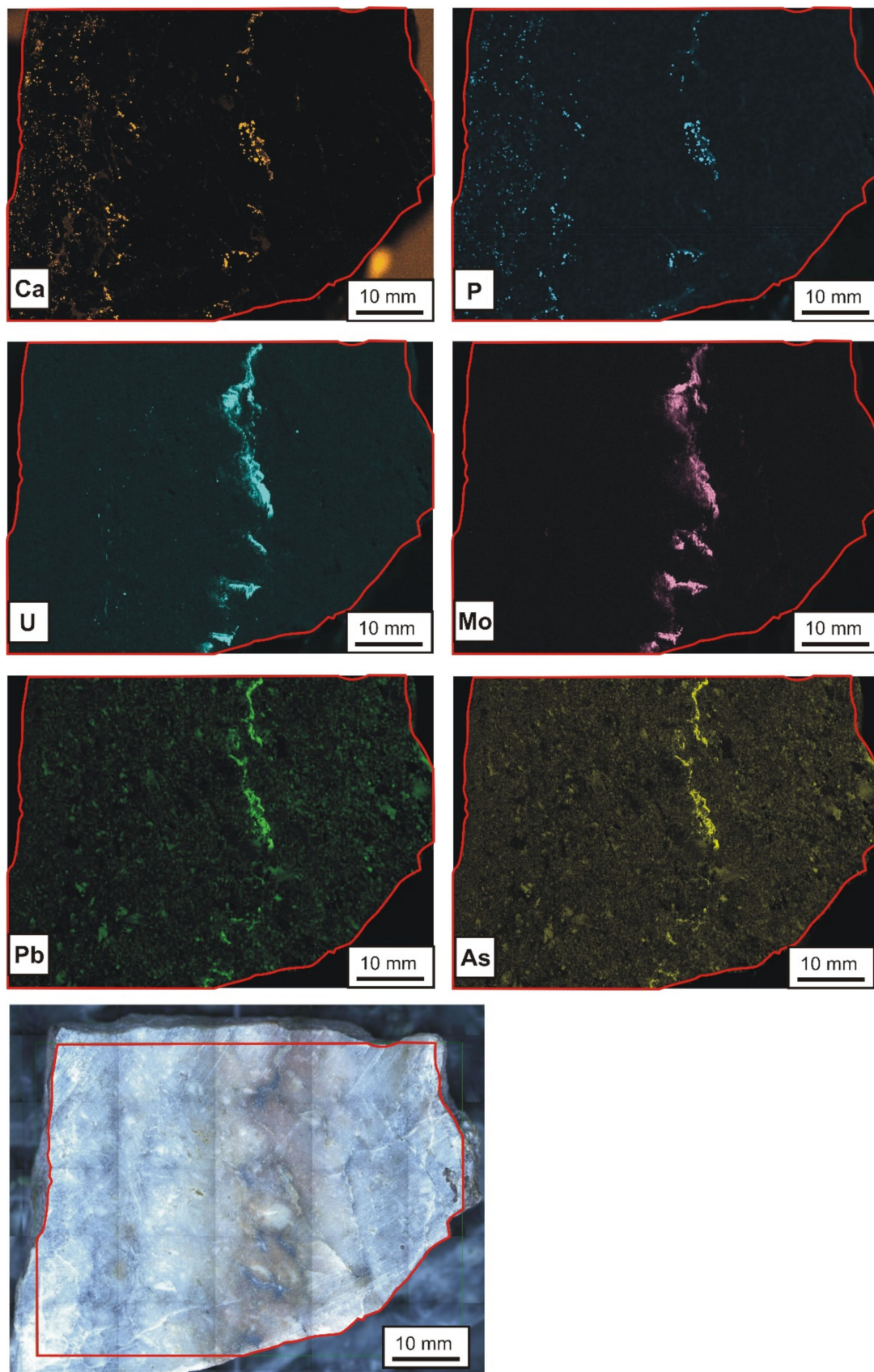


**Figure 3.** XRF distribution maps of selected elements in quartz vein with U-Mo mineralization (bottom subfigure). Ca and P indicate the distribution of accessory fluorapatite in quartz. Photo: S. Milovská.

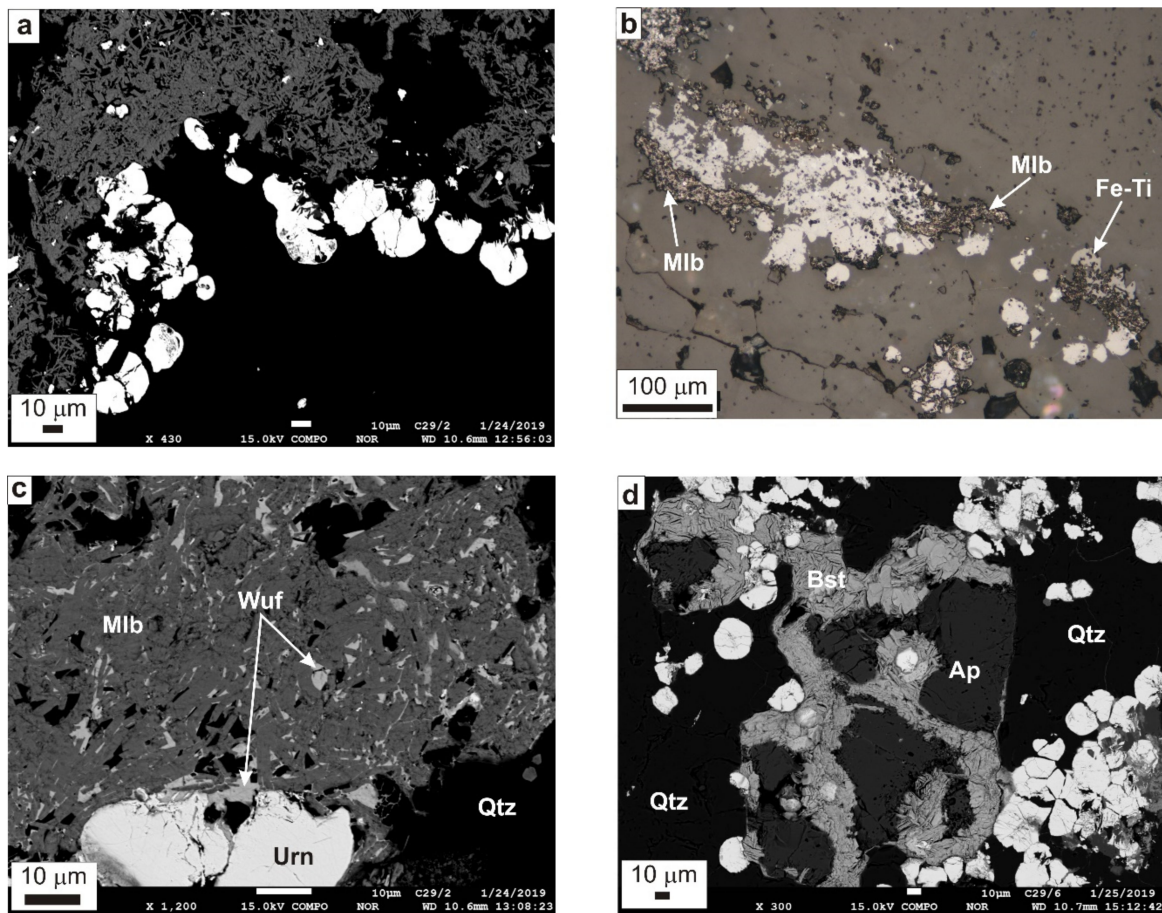


**Figure 4.** (a) Uraninite (white) aggregates on the border of the molybdenite vein (dark grey) and is also enclosed in molybdenite. The quartz is black. (b) Accumulation of uraninite (light grey) rimmed by fine-grained molybdenite (Mlb). At the bottom right are Fe-Ti oxides (Fe-Ti). The surroundings are quartz (dark grey). (c) Cavities and cracks in molybdenite (Mlb) aggregate are partially filled by wulfenite (Wuf), which also partially rims uraninite globules (Urn). The surrounding phase is quartz (Qtz). (d) Fluorapatite (Ap) is accompanied by uraninite (white). Supergene uranyl mineral, bassetite (Bst), encloses both minerals and also fills cracks in fluorapatite. The host mineral is quartz (Qtz). Pictures a, c, d—BSE (photo: T. Mikuš); picture b—reflected light, PPL (photo: Š. Ferenc).

The chemical analyses of the uraninite from Čučma are given in Table 2. The uranium content is relatively high and stable (0.86–0.87 *apfu* of U), indicating that uraninite was practically unaffected by younger hydrothermal processes. Similarly, the low Si content (reaching up to 1.54 wt. % SiO<sub>2</sub>; 0.07 *apfu* of Si) excludes the possibility of its later coiffinitization. Thorium concentrations are very low, under the detection limit of the electron microprobe. From the other elements, the contents of Pb (2.77–3.12 wt. % PbO; a maximum of 0.04 *apfu* of Pb) and Ca (up to 0.82 wt. % CaO; 0.04 *apfu* of Ca) are relatively significantly increased. Y + REE are present in the uraninite (2.99–4.54 wt. % Y<sub>2</sub>O<sub>3</sub> + REE<sub>2</sub>O<sub>3</sub>; 0.05–0.07 *apfu* of Y + REE), while the ratio of LREE (with an average of 0.03 *apfu*) and HREE (with an average of 0.02 *apfu*) is relatively equal (with a moderate predominance of LREE). The content of yttrium is ranging from 0.41 to 0.77 wt. % Y<sub>2</sub>O<sub>3</sub> (0.03–0.04 *apfu* of Y). The content of other elements does not have a significant effect on the variations of the uraninite chemical composition.

**Table 2.** Representative WDS microanalyses of uraninite from Čučma (Majerská valley).

	1	2	3	4	5	6	7	8	9	10	11	12	13	14
UO <sub>2</sub>	88.64	89.20	88.90	89.58	89.04	89.64	88.89	90.42	88.95	88.73	88.98	89.47	89.25	89.92
CaO	0.57	0.54	0.70	0.67	0.56	0.63	0.70	0.67	0.82	0.75	0.50	0.69	0.60	0.67
FeO	0.01	0.00	0.00	0.00	0.02	0.00	0.00	0.00	0.09	0.00	0.00	0.00	0.00	0.00
PbO	3.08	3.11	3.08	3.09	3.08	3.10	3.07	3.09	2.77	3.02	3.08	3.12	3.04	3.05
Al <sub>2</sub> O <sub>3</sub>	0.12	0.08	0.08	0.08	0.13	0.10	0.08	0.11	0.05	0.12	0.09	0.07	0.12	0.05
Y <sub>2</sub> O <sub>3</sub>	0.42	0.55	0.61	0.64	0.34	0.58	0.64	0.56	0.77	0.54	0.59	0.65	0.41	0.71
La <sub>2</sub> O <sub>3</sub>	0.00	0.00	0.00	0.00	0.00	0.00	0.00	0.00	0.00	0.03	0.00	0.00	0.00	0.00
Ce <sub>2</sub> O <sub>3</sub>	0.23	0.24	0.24	0.23	0.31	0.27	0.21	0.22	0.34	0.28	0.34	0.30	0.25	0.23
Pr <sub>2</sub> O <sub>3</sub>	0.32	0.39	0.33	0.32	0.28	0.39	0.36	0.40	0.33	0.27	0.31	0.31	0.31	0.35
Nd <sub>2</sub> O <sub>3</sub>	0.16	0.17	0.21	0.18	0.02	0.15	0.21	0.19	0.26	0.16	0.19	0.23	0.14	0.22
Sm <sub>2</sub> O <sub>3</sub>	0.21	0.26	0.30	0.34	0.22	0.26	0.25	0.23	0.36	0.28	0.27	0.28	0.20	0.25
Eu <sub>2</sub> O <sub>3</sub>	0.30	0.35	0.30	0.35	0.30	0.37	0.31	0.31	0.36	0.27	0.31	0.36	0.35	0.41
Gd <sub>2</sub> O <sub>3</sub>	0.30	0.26	0.35	0.38	0.28	0.41	0.36	0.37	0.44	0.34	0.33	0.37	0.29	0.39
Tb <sub>2</sub> O <sub>3</sub>	0.12	0.09	0.08	0.14	0.09	0.09	0.05	0.09	0.14	0.10	0.11	0.09	0.15	0.17
Dy <sub>2</sub> O <sub>3</sub>	0.18	0.18	0.28	0.29	0.16	0.22	0.26	0.25	0.35	0.25	0.21	0.28	0.20	0.30
Ho <sub>2</sub> O <sub>3</sub>	0.09	0.07	0.03	0.05	0.03	0.15	0.10	0.00	0.03	0.00	0.07	0.04	0.09	0.06
Er <sub>2</sub> O <sub>3</sub>	0.56	0.70	0.64	0.59	0.58	0.65	0.54	0.57	0.60	0.63	0.60	0.61	0.53	0.59
Tm <sub>2</sub> O <sub>3</sub>	0.12	0.10	0.13	0.14	0.12	0.09	0.12	0.15	0.10	0.10	0.12	0.16	0.13	0.15
Yb <sub>2</sub> O <sub>3</sub>	0.26	0.34	0.30	0.37	0.23	0.33	0.32	0.34	0.36	0.28	0.33	0.28	0.28	0.30
Lu <sub>2</sub> O <sub>3</sub>	0.10	0.14	0.15	0.08	0.04	0.10	0.13	0.19	0.12	0.07	0.17	0.18	0.19	0.10
SiO <sub>2</sub>	1.43	1.05	1.09	0.95	1.54	1.05	0.98	1.30	0.73	1.39	1.21	0.92	1.35	0.77
P <sub>2</sub> O <sub>5</sub>	0.04	0.04	0.04	0.04	0.07	0.06	0.04	0.05	0.04	0.06	0.04	0.05	0.06	0.04
As <sub>2</sub> O <sub>5</sub>	0.16	0.15	0.15	0.16	0.18	0.15	0.16	0.15	0.16	0.16	0.15	0.16	0.16	0.15
SO <sub>3</sub>	0.02	0.01	0.01	0.02	0.00	0.00	0.00	0.03	0.04	0.00	0.00	0.01	0.02	0.02
Total wt. %	97.44	98.01	98.00	98.68	97.61	98.80	97.78	99.69	98.19	97.81	97.99	98.63	98.10	98.87
Y + REE wt. %	3.36	3.82	3.95	4.09	2.99	4.06	3.86	3.86	4.54	3.59	3.94	4.16	3.51	4.21
empirical formula (calculation on basis of 2 oxygens)														
U	0.855	0.868	0.861	0.866	0.855	0.863	0.867	0.855	0.866	0.852	0.861	0.867	0.857	0.874
Ca	0.027	0.026	0.033	0.031	0.026	0.029	0.033	0.030	0.038	0.035	0.023	0.032	0.028	0.031
Fe	0.000	0.000	0.000	0.000	0.001	0.000	0.000	0.000	0.003	0.000	0.000	0.000	0.000	0.000
Pb	0.036	0.037	0.036	0.036	0.036	0.036	0.036	0.035	0.033	0.035	0.036	0.037	0.035	0.036
Al	0.006	0.004	0.004	0.004	0.006	0.005	0.004	0.006	0.002	0.006	0.005	0.004	0.006	0.003
Y	0.010	0.013	0.014	0.015	0.008	0.013	0.015	0.013	0.018	0.012	0.014	0.015	0.009	0.016
La	0.000	0.000	0.000	0.000	0.000	0.000	0.000	0.000	0.000	0.000	0.000	0.000	0.000	0.000
Ce	0.004	0.004	0.004	0.004	0.005	0.004	0.003	0.003	0.005	0.004	0.005	0.005	0.004	0.004
Pr	0.005	0.006	0.005	0.005	0.004	0.006	0.006	0.006	0.005	0.004	0.005	0.005	0.005	0.006
Nd	0.002	0.003	0.003	0.003	0.000	0.002	0.003	0.003	0.004	0.002	0.003	0.004	0.002	0.003
Sm	0.003	0.004	0.004	0.005	0.003	0.004	0.004	0.003	0.005	0.004	0.004	0.004	0.003	0.004
Eu	0.004	0.005	0.004	0.005	0.004	0.005	0.005	0.005	0.005	0.004	0.005	0.005	0.005	0.006
Gd	0.004	0.004	0.005	0.005	0.004	0.006	0.005	0.005	0.006	0.005	0.005	0.005	0.004	0.006
Tb	0.002	0.001	0.001	0.002	0.001	0.001	0.001	0.001	0.002	0.001	0.002	0.001	0.002	0.003
Dy	0.002	0.002	0.004	0.004	0.002	0.003	0.004	0.003	0.005	0.004	0.003	0.004	0.003	0.004
Ho	0.001	0.001	0.000	0.001	0.000	0.002	0.001	0.000	0.000	0.000	0.001	0.001	0.001	0.001
Er	0.008	0.010	0.009	0.008	0.008	0.009	0.007	0.008	0.008	0.008	0.008	0.008	0.007	0.008
Tm	0.002	0.001	0.002	0.002	0.002	0.001	0.002	0.002	0.001	0.001	0.002	0.002	0.002	0.002
Yb	0.003	0.005	0.004	0.005	0.003	0.004	0.004	0.004	0.005	0.004	0.004	0.004	0.004	0.004
Lu	0.001	0.002	0.002	0.001	0.001	0.001	0.002	0.002	0.002	0.001	0.002	0.002	0.002	0.001
Si	0.062	0.046	0.047	0.041	0.066	0.045	0.043	0.055	0.032	0.060	0.052	0.040	0.058	0.034
P	0.002	0.002	0.002	0.001	0.003	0.002	0.001	0.002	0.002	0.002	0.002	0.002	0.002	0.001
As	0.004	0.004	0.004	0.004	0.004	0.003	0.004	0.003	0.004	0.004	0.003	0.004	0.004	0.003
S	0.001	0.000	0.000	0.001	0.000	0.000	0.000	0.001	0.001	0.000	0.000	0.000	0.001	0.000
Y + REE	0.052	0.060	0.062	0.065	0.046	0.064	0.062	0.059	0.073	0.056	0.062	0.066	0.054	0.067
LREE	0.023	0.026	0.026	0.027	0.021	0.028	0.026	0.026	0.032	0.024	0.027	0.028	0.023	0.028
HREE	0.019	0.022	0.022	0.023	0.017	0.022	0.021	0.021	0.023	0.019	0.022	0.022	0.021	0.023

All uranium is considered to be tetravalent.

*The chemical in situ electron-microprobe U-Pb dating of uraninite* (according to [29]) provided an age interval of between 241 and 269 ± 2 Ma (2 samples, 23-point analyses; Table 3). However, the majority of the age data obtained (22-point analyses) fall into the range of 261–269 ± 2 Ma (with an average of 265 ± 2 Ma), corresponding to the Guadalupian Epoch of Permian.

**Table 3.** Chemical ages of uraninite from Čučma (Majerská valley) calculated according to procedure of Montel et al. [29].

	Sample	Pb meas.	Th wt. %	U wt. %	Pb wt. %	Y wt. %	U <sub>corr.</sub>	Pb <sub>corr.</sub>	Th 2σ	U 2σ	Pb 2σ	U at. %	Pb at. %	Age (Ma)	1σ
1	C29-6	2.8617	blld	78.1362	2.9151	0.3276	75.7921	2.9058	0	0.2715	0.0234	95.9646	4.0354	268	2.3
2	C29-6	2.8862	blld	78.6259	2.9395	0.4301	76.2671	2.9298	0	0.2726	0.0236	95.9568	4.0432	268	2.3
3	C29-6	2.8628	blld	78.3653	2.9156	0.4793	76.0143	2.9058	0	0.2718	0.0233	95.9757	4.0243	267	2.3
4	C29-6	2.8746	blld	78.9599	2.9277	0.5013	76.5911	2.9178	0	0.2735	0.0235	95.9892	4.0108	266	2.3
5	C29-6	2.8707	blld	78.8515	2.9238	0.4952	76.4860	2.9138	0	0.2731	0.0234	95.9890	4.0110	266	2.3
6	C29-6	2.8577	blld	78.4893	2.9116	0.2694	76.1346	2.9024	0	0.2725	0.0233	95.9870	4.0130	266	2.3
7	C29-6	2.8826	blld	79.0197	2.9360	0.4603	76.6491	2.9262	0	0.2735	0.0236	95.9810	4.0190	267	2.3
8	C29-6	2.8700	blld	78.5859	2.9231	0.4610	76.2283	2.9133	0	0.2725	0.0235	95.9767	4.0233	267	2.3
9	C29-6	2.8542	blld	78.3536	2.9069	0.5019	76.0030	2.8969	0	0.2720	0.0234	95.9869	4.0131	266	2.3
10	C29-6	2.8105	blld	78.5054	2.8634	0.4521	76.1502	2.8537	0	0.2724	0.0231	96.0530	3.9470	262	2.3
11	C29-2	2.8083	blld	78.4629	2.8613	0.4380	76.1090	2.8516	0	0.2723	0.0231	96.0538	3.9462	262	2.3
12	C29-2	2.8682	blld	79.7079	2.9221	0.4409	77.3167	2.9124	0	0.2757	0.0235	96.0334	3.9666	263	2.3
13	C29-2	2.5789	blld	78.4052	2.6304	0.6066	76.0530	2.6202	0	0.2719	0.0215	96.3633	3.6367	241	2.1
14	C29-2	2.8355	blld	78.7048	2.8888	0.4129	76.3437	2.8792	0	0.2728	0.0233	96.0285	3.9715	264	2.3
15	C29-2	2.8035	blld	78.2172	2.8563	0.4273	75.8707	2.8466	0	0.2717	0.0231	96.0482	3.9518	262	2.3
16	C29-2	2.8910	blld	78.8949	2.9444	0.4444	76.5281	2.9347	0	0.2734	0.0237	95.9637	4.0363	268	2.3
17	C29-2	2.8649	blld	78.4324	2.9179	0.4630	76.0794	2.9081	0	0.2722	0.0235	95.9762	4.0238	267	2.3
18	C29-2	2.8956	blld	78.8696	2.9487	0.5106	76.5035	2.9387	0	0.2733	0.0237	95.9565	4.0435	268	2.3
19	C29-2	2.8202	blld	78.6703	2.8739	0.3232	76.3102	2.8646	0	0.2729	0.0231	96.0469	3.9531	262	2.3
20	C29-2	2.8051	blld	78.7543	2.8580	0.4814	76.3917	2.8482	0	0.2731	0.0229	96.0724	3.9276	261	2.2
21	C29-2	2.8504	blld	78.3925	2.9031	0.5135	76.0407	2.8931	0	0.2721	0.0234	95.9939	4.0061	266	2.3
22	C29-2	2.8345	blld	79.2638	2.8874	0.5555	76.8859	2.8773	0	0.2743	0.0233	96.0579	3.9421	262	2.3
23	C29-2	2.8850	blld	78.4314	2.9380	0.4641	76.0785	2.9282	0	0.2721	0.0235	95.9490	4.0510	269	2.3

C29-2: weighted average of age (263 Ma); C29-6: weighted average of age (266 Ma); C29-2 and C29-6: weighted average of age (265 Ma); blld: below lower limit of detection.

Unspecified, non-stoichiometric *U-Ti oxides* are present only infrequently as irregular, metamict aggregates up to 0.15 mm in size, partially intergrown with molybdenite and uraninite (Figure 5a). Leucoxenized *Fe-Ti oxides*, without uranium occur in similar positions.

*Pyrite* is a frequent mineral. It was found in association with uraninite, molybdenite, minerals of the kobellite–tintinaite series, sulphotellurides and ullmannite. Pyrite (I) forms irregular to botryoidal aggregates up to 5 mm in size without chemical zoning in quartz. It grows on uraninite globules and encloses (?) grains of joséite-B. Minerals of the kobellite–tintinaite series grow on its aggregates (Figure 5b). Veinlets of pyrite II (distinct chemical zoning) cut accumulations of molybdenite and kobellite–tintinaite series minerals (Figure 5c). Pyrite is, to a great extent, intimately replaced by supergene oxide minerals (or their mixture), which is reflected in the low totals of microprobe analyses (Table 4) and varying ratios of cations and sulphur (0.51–0.60). The high susceptibility of pyrite to weathering processes can most likely be explained by its instability, caused by the significantly increased contents of Bi (0.01–0.07 *apfu*), Sb (0.01–0.06 *apfu*), Pb (up to 0.01 *apfu*) and Cu (up to 0.01 *apfu*) in the original (not weathered) mineral phase.

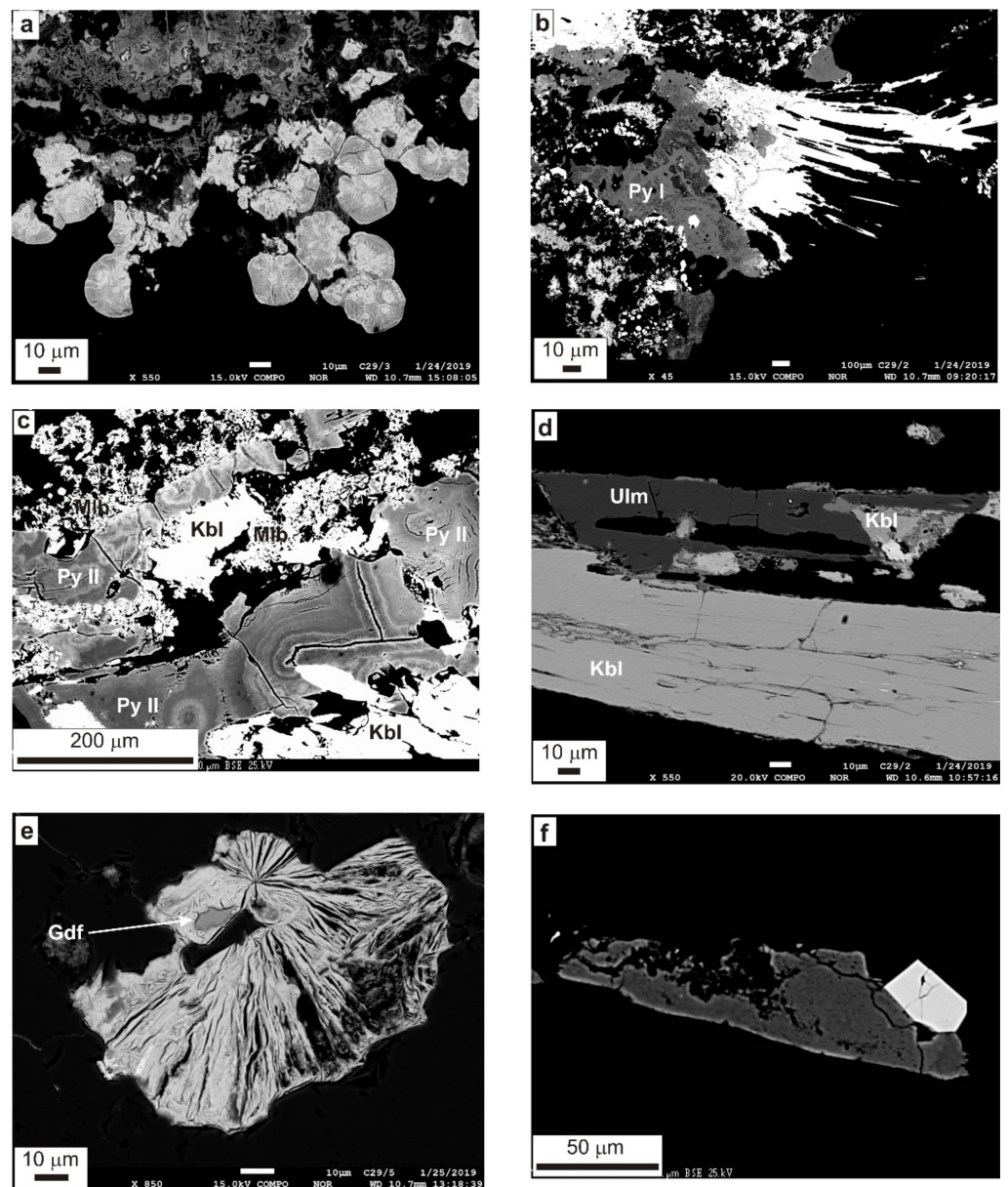


**Figure 5.** (a) Globular aggregates of uraninite (white) that are intensively replaced by an unidentified supergene uranyl mineral (light grey) in contact with the U-Ti oxides (tones of dark grey, top of the picture). (b) Pyrite I (Py I) overgrown by kobellite, uraninite, molybdenite, sulphotellurides and other ore minerals (white). (c) Veinlets of zonal pyrite II (Py II) cutting accumulations of molybdenite (Mlb) and kobellite–tintinaite series minerals (Kbl). (d) Kobellite (Kbl) in contact with ullmannite (Ulm). Ullmannite is overgrown and replaced with kobellite and joséite-B (white). Quartz is black. (e) Relic of gersdorffite (Gdf) overgrown by zeunerite (light grey) in a quartz cavity (black). (f) Cobaltite (white) and pyrite (dark grey) in quartz. BSE, photos by T. Mikuš (a,b,d,e) and M. Števkó (c,f).

*Ullmannite* is a rare mineral. It was found in close spatial association with kobellite in the form of elongated grains, up to 0.2 mm in size (Figure 5d). Ullmannite is usually replaced and overgrown by kobellite, joséite-B and supergene Pb-Bi-Sb oxides. The chemical composition of ullmannite is relatively monotonous and its calculated empirical formula is close to the ideal composition of this mineral (Table 5). Only slightly increased contents of Bi and Se (both below 0.01 *apfu*) were detected in studied ullmannite.

**Table 4.** Chemical composition of pyrite from Čučma (Majerská valley).

	1	2	3	4	5
Fe	35.36	37.47	37.72	40.29	42.34
Ni	0.11	0.09	0.11	0.07	0.08
Cu	0.27	0.35	0.34	0.25	0.33
Pb	0.6	0.78	0.58	0.5	0.65
Sb	4.37	3.07	3.16	1.33	0.76
Bi	9.91	6.9	7.19	3.36	2.11
S	38.59	42.6	42.31	47.07	48.51
Total wt. %	89.21	91.26	91.41	92.87	94.78
Empirical formula (on basis of the 3 atoms)					
Fe	0.985	0.973	0.981	0.973	0.990
Ni	0.003	0.002	0.003	0.002	0.002
Cu	0.007	0.008	0.008	0.005	0.007
Pb	0.005	0.005	0.004	0.003	0.004
Sb	0.056	0.037	0.038	0.015	0.008
Bi	0.074	0.048	0.050	0.022	0.013
Σ	1.128	1.073	1.083	1.020	1.024
S	1.872	1.927	1.917	1.980	1.976
Cat./S	0.60	0.56	0.57	0.51	0.52

**Table 5.** Representative WDS microanalyses of ullmannite from Čučma (Majerská valley).

	1	2	3
Ni	27.21	27.43	27.46
Co	0.05	0.09	0.03
Fe	0.04	0.03	0.04
As	0.00	0.07	0.01
Sb	56.20	56.00	55.92
Bi	0.12	0.08	0.17
Se	0.05	0.03	0.12
S	14.42	14.48	14.85
Total wt. %	98.09	98.21	98.59
Empirical formula (on basis of 3 atoms)			
Ni	1.009	1.014	1.007
Co	0.002	0.003	0.001
Fe	0.001	0.001	0.002
As	0.000	0.002	0.000
Sb	1.005	0.998	0.988
Bi	0.001	0.001	0.002
Se	0.001	0.001	0.003
S	0.980	0.980	0.997

*Gersdorffite* was found only in one case. It forms an irregular grain, about 10 µm in size, overgrown with the supergene uranyl arsenate - zeunerite (Figure 5e), in quartz cavity. The chemical composition of gersdorffite was verified only by non-standardized EDS analysis.

*Cobaltite* occurs only rarely as individual, euhedral to subhedral crystals up to 30 µm in size, either enclosed in quartz or growing over pyrite (Figure 5f). The quantitative chemical analyses of cobaltite are shown in Table 6. The two compositional varieties of cobaltite were distinguished (Figure 6) with the following average empirical formulae:  $(\text{Co}_{0.57}\text{Ni}_{0.22}\text{Fe}_{0.20})_{\Sigma 0.99}\text{As}_{0.98}\text{S}_{1.02}$  and  $(\text{Co}_{0.80}\text{Fe}_{0.14}\text{Ni}_{0.06})_{\Sigma 1.00}\text{As}_{0.90}\text{S}_{1.10}$ .

**Table 6.** Representative WDS microanalyses of cobaltite from Čučma (Majerská valley).

	1	2	3	4	5	6	7	8
Fe	4.94	4.48	4.48	4.30	5.63	7.12	6.46	6.57
Co	28.10	27.69	29.70	29.39	29.43	18.95	20.86	21.21
Ni	2.19	2.90	2.20	2.33	1.21	8.80	7.55	7.26
As	41.96	42.17	41.43	41.81	40.13	44.60	44.33	44.32
S	21.85	21.22	21.38	21.25	22.28	19.63	19.61	19.78
Total wt. %	99.05	98.46	99.19	99.08	98.68	99.10	98.81	99.14
Empirical formula (on basis of the 3 atoms)								
Fe	0.144	0.132	0.131	0.126	0.163	0.212	0.193	0.195
Co	0.776	0.773	0.821	0.815	0.809	0.534	0.589	0.597
Ni	0.061	0.081	0.061	0.065	0.033	0.249	0.214	0.205
Σ	0.980	0.986	1.013	1.005	1.006	0.995	0.996	0.997
As	0.911	0.926	0.901	0.912	0.868	0.989	0.985	0.981
S	1.109	1.089	1.086	1.083	1.126	1.017	1.019	1.023
Σ	2.020	2.014	1.987	1.995	1.994	2.005	2.004	2.003

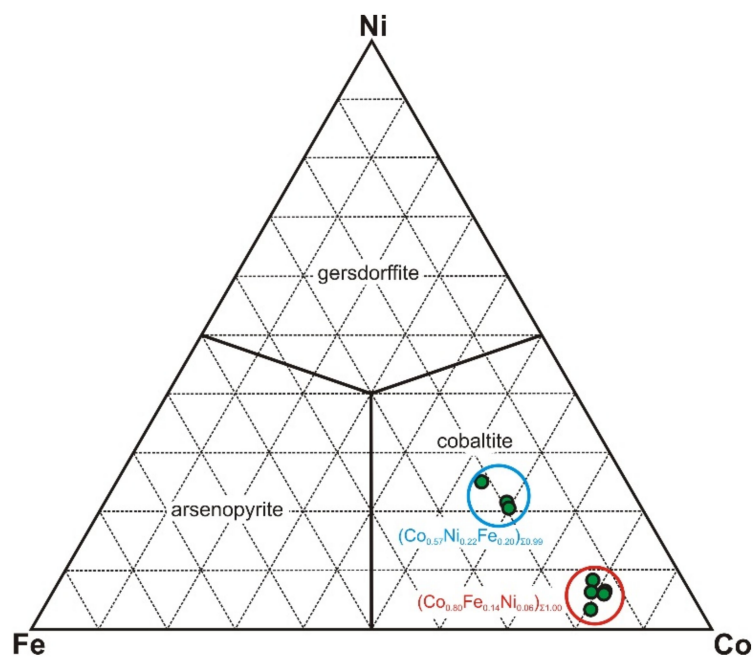


**Figure 6.** Chemical composition of cobaltite from Čučma in ternary system Fe-Co-Ni.

*Tetradymite* was found in only one case. It forms an irregular grain (0.3 mm in size) in close spatial association with molybdenite, uraninite, titanite and chlorite (Figure 7a). The chemical composition of tetradymite is relatively stable (Table 7, Figure 8), containing only minor amounts of Sb (about 0.06 *apfu*), Pb (up to 0.01 *apfu*) and Se (with a maximum of 0.03 *apfu*). The average empirical formula of the tetradymite from Čučma based on five atoms is  $(\text{Bi}_{2.03}\text{Sb}_{0.06}\text{Pb}_{0.01})_{\Sigma 2.10}\text{Te}_{1.92}(\text{S}_{0.96}\text{Se}_{0.02})_{\Sigma 0.98}$ .

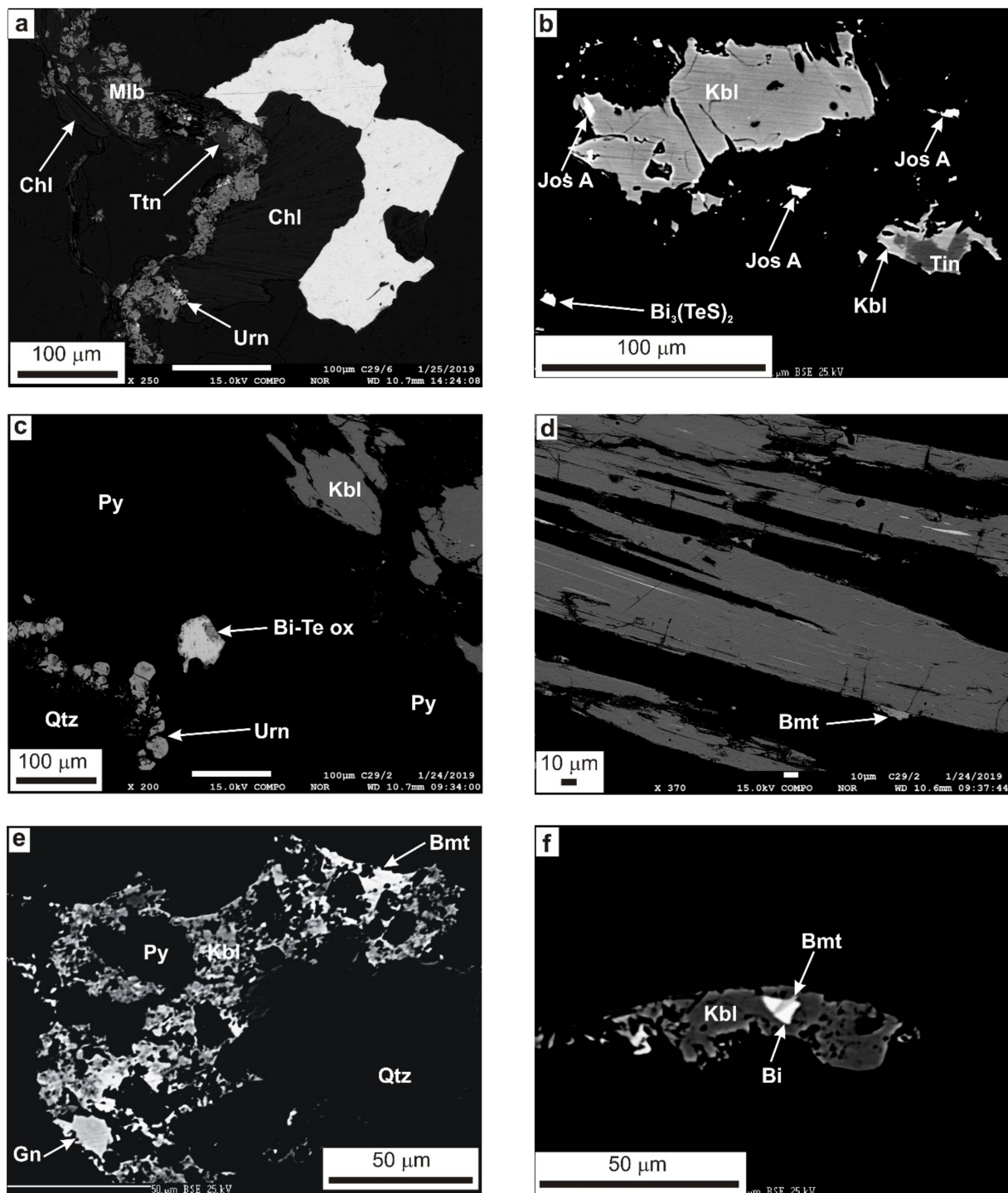


**Figure 7.** (a) Tetradytmite aggregate (white) in spatial association with chlorite (Chl), titanite (Ttn), molybdenite (Mlb) and uraninite (Urn). The host mineral is quartz (black). (b) Aggregates of kobellite–tintinaite series minerals (Kbl and Tin, respectively) accompanied by josite-A (Jos A) and  $\text{Bi}_3(\text{TeS})_2$  mineral phase (“protojosite”) in quartz (black). (c) Grain of josite-B (white), rimmed by Bi-Te oxides (Bi-Te ox) in pyrite I (Py). In the top right are grains of minerals of the kobellite–tintinaite series (Kbl), and in the bottom left is a pyrite aggregate lined with uraninite (Urn). To the left of uraninite is quartz (Qtz). (d) Needle-like crystals of kobellite–tintinaite (dark grey) with lamellae of the nameless  $\text{Bi}_3(\text{Te,S})_2$  mineral phase (white) corresponding to the “protojosite”. Bismuthinite (Bmt) is grown on kobellite–tintinaite crystals. (e) Pyrite (Py) and galena (Gn) are enclosed by kobellite–tintinaite series minerals (Kbl), which overgrows with bismuthinite (Bmt) in quartz (Qtz). (f) Bismuthinite (Bmt) overgrown by bismuth (Bi); both are enclosed in kobellite–tintinaite series minerals. Host mineral is quartz (black). BSE, photos by T. Mikuš (a,c,d) and M. Števkó (b,e,f).

**Table 7.** Chemical composition of tetradyomite (an. 1–3), joséite-A (an. 4–8), joséite-B (an. 9–11) and “protojoséite”, Bi<sub>3</sub>(TeS)<sub>2</sub>, (an. 12–14) from Čučma (Majerská valley).

	1	2	3	4	5	6	7	8	9	10	11	12	13	14
Bi	59.64	59.76	59.07	77.84	78.66	78.73	79.51	79.56	75.01	74.34	75.10	71.06	72.41	72.27
Sb	0.82	1.04	1.01	0.53	0.29	0.29	0.29	0.29	0.40	0.43	0.36	1.96	0.55	0.65
Fe	0.00	0.01	0.00	0.46	0.70	0.24	0.05	0.06	0.19	0.28	0.22	0.09	0.00	0.00
Cu	0.00	0.00	0.00	0.08	0.00	0.00	0.00	0.07	0.00	0.00	0.00	0.23	0.44	0.47
In				0.06	0.00	0.09	0.08	0.00					0.00	0.06
Pb	0.00	0.19	0.32	1.60	1.17	0.93	1.44	1.45	0.98	1.04	1.38	2.28	2.84	2.80
Te	34.14	34.03	34.63	11.74	11.96	11.99	12.18	11.95	21.56	21.75	21.49	17.86	17.89	17.31
S	4.22	4.44	4.34	6.13	5.96	6.58	6.07	6.12	2.63	2.68	2.75	4.32	3.44	3.70
Se	0.26	0.20	0.30	1.00	0.91	1.09	0.90	0.85	0.09	0.20	0.19	1.07	1.13	1.05
Total wt. %	99.08	99.67	99.66	99.44	99.65	99.94	100.52	100.35	100.87	100.71	101.50	98.85	98.70	98.31
Empirical formulae														
Bi	2.054	2.033	2.011	3.776	3.829	3.758	3.873	3.876	4.036	3.980	3.996	2.575	2.734	2.715
Sb	0.048	0.061	0.059	0.044	0.024	0.024	0.024	0.024	0.037	0.040	0.033	0.122	0.035	0.042
Fe	0.000	0.001	0.000	0.084	0.128	0.043	0.009	0.011	0.039	0.055	0.045	0.012	0.000	0.000
Cu	0.000	0.000	0.000	0.013	0.000	0.000	0.000	0.011	0.000	0.000	0.000	0.027	0.055	0.058
In				0.005	0.000	0.008	0.007	0.000					0.000	0.004
Pb	0.000	0.007	0.011	0.078	0.057	0.045	0.071	0.071	0.053	0.056	0.074	0.083	0.108	0.106
Σ	2.103	2.102	2.081	4.000	4.038	3.877	3.985	3.994	4.165	4.131	4.148	2.819	2.933	2.925
Te	1.926	1.896	1.930	0.933	0.953	0.937	0.972	0.953	1.900	1.907	1.873	1.060	1.106	1.065
S	0.948	0.984	0.962	1.939	1.891	2.047	1.928	1.943	0.922	0.934	0.952	1.019	0.848	0.906
Se	0.024	0.018	0.027	0.128	0.117	0.138	0.116	0.110	0.013	0.028	0.026	0.103	0.113	0.104
Σ	0.972	1.002	0.988	2.067	2.008	2.185	2.044	2.053	0.935	0.962	0.979	1.122	0.961	1.010

Empirical formulae were calculated on the basis of 5 atoms (tetradyomite, Bi<sub>3</sub>(TeS)<sub>2</sub> phase) and 7 atoms (joséite A, B).

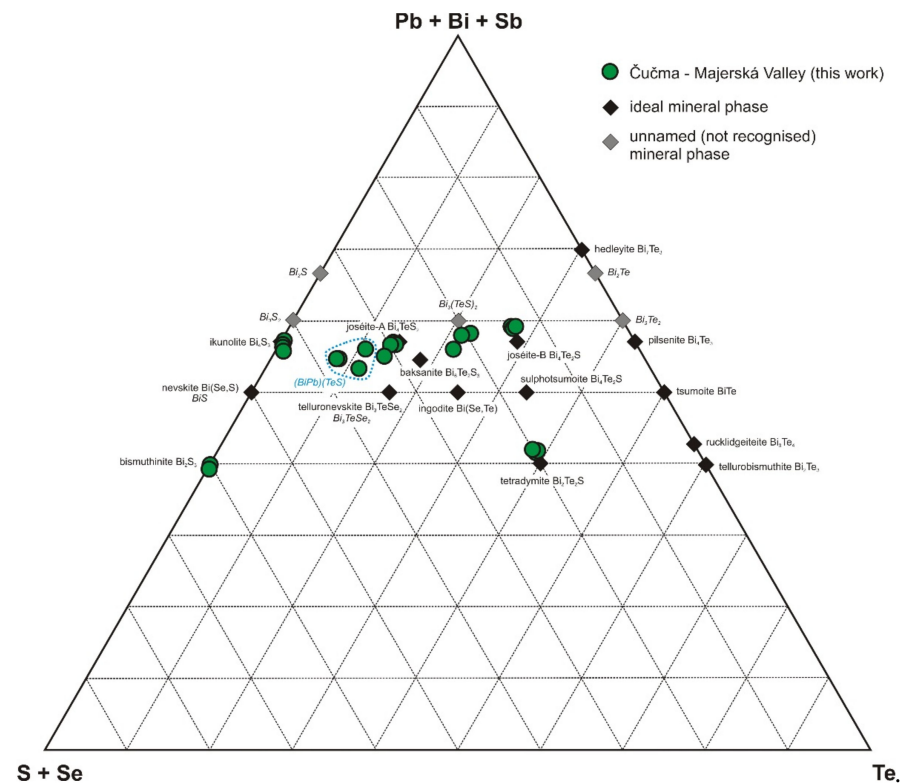


**Figure 8.** Chemical composition of the sulphotellurides, ikonolite and bismuthinite from Čučma in ternary system S + Se-Te-Pb + Bi + Sb.

**Joséite-A** is relatively common as anhedral grains up to 10  $\mu\text{m}$ , enclosed in pyrite together with minerals of kobellite–tintinaite series (Figure 7b). The chemical composition of the studied Joséite-A is close to the ideal composition of this mineral phase (Table 7, Figure 8). The most important admixture in the Joséite-A from Čučma is the content of Pb, ranging from 0.93 to 1.60 wt. % (0.05–0.08 *apfu*). Minor amounts of antimony (on average, 0.34 wt. %; 0.03 *apfu*) and iron (up to 0.70 wt. %; 0.13 *apfu*) were also detected. The anionic position is characterized by the stable presence of Se (with an average of 0.95 wt. %; 0.12 *apfu*). The average chemical composition of the studied Joséite-A is  $(\text{Bi}_{3.82}\text{Pb}_{0.06}\text{Fe}_{0.05}\text{Sb}_{0.03})_{\Sigma 3.96}\text{Te}_{0.95}(\text{S}_{1.95}\text{Se}_{0.12})_{\Sigma 2.07}$ .

**Joséite-B** was rarely found in association with uraninite, pyrite and minerals of the kobellite–tintinaite series (Figure 7c). It forms individual grains (up to 0.05 mm in size) in pyrite, rimmed by an unspecified supergene Bi-Te oxidic mineral phase. The studied mineral phase has a relatively monotonous chemical composition, which is close to the ideal formula,  $\text{Bi}_4\text{Te}_2\text{S}$  (Table 7, Figure 8). Only minor contents of Sb (with an average of 0.40 wt. %; 0.04 *apfu*), Pb (with an average of 1.13 wt. %; 0.06 *apfu*) and Fe (up to 0.23 wt. %; 0.05 *apfu*) were observed in the Joséite-B from Čučma. In the anionic position, S is replaced by a minor content of Se (up to 0.20 wt. %; 0.03 *apfu*). The average chemical composition of the studied Joséite-B can be expressed as  $(\text{Bi}_{4.00}\text{Pb}_{0.06}\text{Fe}_{0.05}\text{Sb}_{0.04})_{\Sigma 4.15}\text{Te}_{1.89}(\text{S}_{0.94}\text{Se}_{0.02})_{\Sigma 0.96}$ .

**An Unnamed  $\text{Bi}_3(\text{Te},\text{S})_2$  mineral phase** forms a thin lamellae enclosed in minerals of the kobellite–tintinaite series (Figure 7d), or small irregular grains in quartz (Figure 7b). Its chemical composition corresponds to the transitional phase between Joséite-A and Joséite-B and approaches the discredited protojoseite (Table 7, Figure 8). Compared to Joséite-A and B, it has a more significantly increased Pb content (on average, 2.64 wt. %; 0.1 *apfu*) and a slightly increased Sb content (with an average of 1.05 wt. %; 0.07 *apfu*). The average Cu content is 0.38 wt. % (0.05 *apfu*). The Te content is around 17.68 wt. % (1.08 *apfu*). The S content is, on average, 3.82 wt. % (0.92 *apfu*) and the Se content is 1.08 wt. % (0.11 *apfu*). The Te/(S+Se) contents ratio is nearly equal (1.05). The chemical composition of this mineral phase can be expressed as  $(\text{Bi}_{2.67}\text{Pb}_{0.10}\text{Sb}_{0.07}\text{Cu}_{0.05})_{\Sigma 2.89}(\text{Te}_{1.08}\text{S}_{0.92}\text{Se}_{0.11})_{\Sigma 2.11}$ .

**The Unnamed  $(\text{BiPb})(\text{TeS})$  phase** is very rare as tiny inclusions (reaching up to 10  $\mu\text{m}$  in size) enclosed in minerals of the kobellite–tintinaite series. This mineral phase is characterized by variable chemical composition (Table 8, Figure 8). The content of Bi varies in the range of 64.37–71.68 wt. % (0.82–0.9 *apfu*), the content of Sb (1.62–4.13 wt. %; 0.04–0.09 *apfu*) and Pb (6.33–11.40 wt. %; 0.09–0.15 *apfu*) also changes more significantly. A small amount of Cu is stably present (with an average of 0.38 wt. %; 0.02 *apfu*). The content of Te ranges from 7.59 to 10.71 wt. % (0.16–0.22 *apfu*), the S content is in the range of 6.63–8.56 wt. % (0.60–0.70 *apfu*) and the average Se content is 1.40 wt. % (0.05 *apfu*). The  $(\text{Bi} + \text{Sb} + \text{Pb})/(\text{Te} + \text{S} + \text{Se})$  contents ratio is around 1.23. Based on the molar ratios of the elements, the following empirical formula can be proposed for this mineral phase:  $(\text{Bi}_{0.90}\text{Pb}_{0.11}\text{Sb}_{0.08}\text{Cu}_{0.02})_{\Sigma 1.11}(\text{Te}_{0.19}\text{S}_{0.66}\text{Se}_{0.05})_{\Sigma 0.90}$ .

**Ikunolite** is rare and it forms anhedral grains (up to 10  $\mu\text{m}$  in size) enclosed together with kobellite in aggregates of pyrite. The studied ikunolite has a homogenous chemical composition (Table 9, Figure 8), which almost coincides with the ideal formula,  $\text{Bi}_4\text{S}_3$ . In the cationic position, only an insignificantly increased Cu content (up to 0.21 wt. %; 0.03 *apfu*) was detected. The content of other elements is negligible. The anionic position is characterized by the dominance of S (with an average of 10.39 wt. %; 3.01 *apfu*). A minor content of Te is present (up to 0.96 wt. %; 0.07 *apfu*) and the Se content reaches only up to 0.19 wt. % (0.02 *apfu*). The average empirical formula of the ikunolite from Čučma is  $(\text{Bi}_{3.93}\text{Cu}_{0.01})_{\Sigma 3.94}(\text{S}_{3.01}\text{Te}_{0.03}\text{Se}_{0.01})_{\Sigma 3.05}$ .

**Table 8.** Representative WDS microanalyses of unnamed (BiPb)(TeS) mineral phase from Čučma (Majerská valley).

	1	2	3	4
Bi	64.37	70.13	71.34	71.68
Sb	4.13	1.62	3.94	4.01
Fe	0.17	0.17	0.00	0.00
Cu	0.46	0.28	0.37	0.40
In	0.00	0.07	0.00	0.07
Pb	11.40	6.33	7.21	8.11
Te	10.71	9.26	7.73	7.59
S	7.95	6.63	8.31	8.56
Se	1.16	1.49	1.54	1.40
Total wt. %	100.35	95.98	100.44	101.82
Empirical formula (calculated on the basis of 2 atoms)				
Bi	0.817	0.979	0.906	0.895
Sb	0.090	0.039	0.086	0.086
Fe	0.008	0.009	0.000	0.000
Cu	0.019	0.013	0.015	0.016
In	0.000	0.002	0.000	0.002
Pb	0.146	0.089	0.092	0.102
Σ	1.080	1.130	1.100	1.101
Te	0.223	0.212	0.161	0.155
S	0.658	0.603	0.688	0.697
Se	0.039	0.055	0.052	0.046
Σ	0.920	0.870	0.900	0.899

**Table 9.** Chemical composition of bismuth (an. 1), bismuthinite (an. 2–8; A-type: an. 2–3, B-type: an. 4–8) and ikonolite (an. 9–13) from Čučma (Majerská valley).

	1	2	3	4	5	6	7	8	9	10	11	12	13
Bi	98.40	82.77	79.70	64.51	63.16	62.54	63.08	62.96	89.77	87.93	87.48	88.69	88.72
Sb	0.51	0.00	0.01	13.21	13.40	13.44	13.54	13.60	0.00	0.00	0.08	0.00	0.00
Cu	0.30	0.14	0.09	0.49	0.38	0.37	0.40	0.26	0.15	0.21	0.12	0.00	0.00
In							0.00	0.06	0.00	0.00	0.08	0.09	0.07
Pb	0.66	0.66	1.55	1.66	1.26	1.22	1.29	1.05	0.00	0.04	0.04	0.00	0.00
S		18.24	17.67	18.01	19.98	19.81	19.92	20.27	10.35	10.24	10.43	10.52	10.39
Se	0.28	0.00	0.02	0.71	0.74	0.74	0.73	0.27	0.00	0.11	0.19	0.00	0.00
Te		0.00	0.00				0.00	0.00	0.12	0.43	0.96	0.44	0.43
Total wt. %	100.15	101.81	99.04	98.59	98.92	98.12	98.97	98.47	100.27	98.53	98.42	99.30	99.18
Empirical formulae													
Bi	0.968	2.041	2.025	1.538	1.430	1.427	1.429	1.423	3.979	3.935	3.869	3.926	3.949
Sb	0.009	0.000	0.000	0.541	0.521	0.526	0.527	0.528	0.000	0.000	0.006	0.000	0.000
Cu	0.010	0.011	0.007	0.039	0.029	0.028	0.030	0.019	0.022	0.031	0.017	0.000	0.000
In							0.000	0.002	0.000	0.000	0.006	0.007	0.006
Pb	0.007	0.016	0.040	0.040	0.029	0.028	0.030	0.024	0.000	0.002	0.002	0.000	0.000
Σ	0.993	2.069	2.072	2.157	2.008	2.009	2.015	1.997	4.001	3.968	3.901	3.933	3.954
S	0.000	2.931	2.927	2.798	2.948	2.946	2.941	2.987	2.990	2.987	3.007	3.035	3.014
Se	0.007	0.000	0.001	0.045	0.044	0.045	0.044	0.016	0.000	0.013	0.022	0.000	0.000
Te		0.000	0.000	0.000	0.000	0.000	0.000	0.000	0.009	0.032	0.070	0.032	0.031
Σ	0.007	2.931	2.928	2.843	2.992	2.991	2.985	3.003	2.999	3.032	3.099	3.067	3.046
Bi/(Bi+Sb)	0.99	1.00	1.00	0.74	0.73	0.73	0.73	0.73	1.00	1.00	1.00	1.00	1.00

*Bismuthinite* can be divided into two types (A and B), based on the significantly different Sb contents in both types (Table 9). Small grains (up to 20 μm in size) of bis-

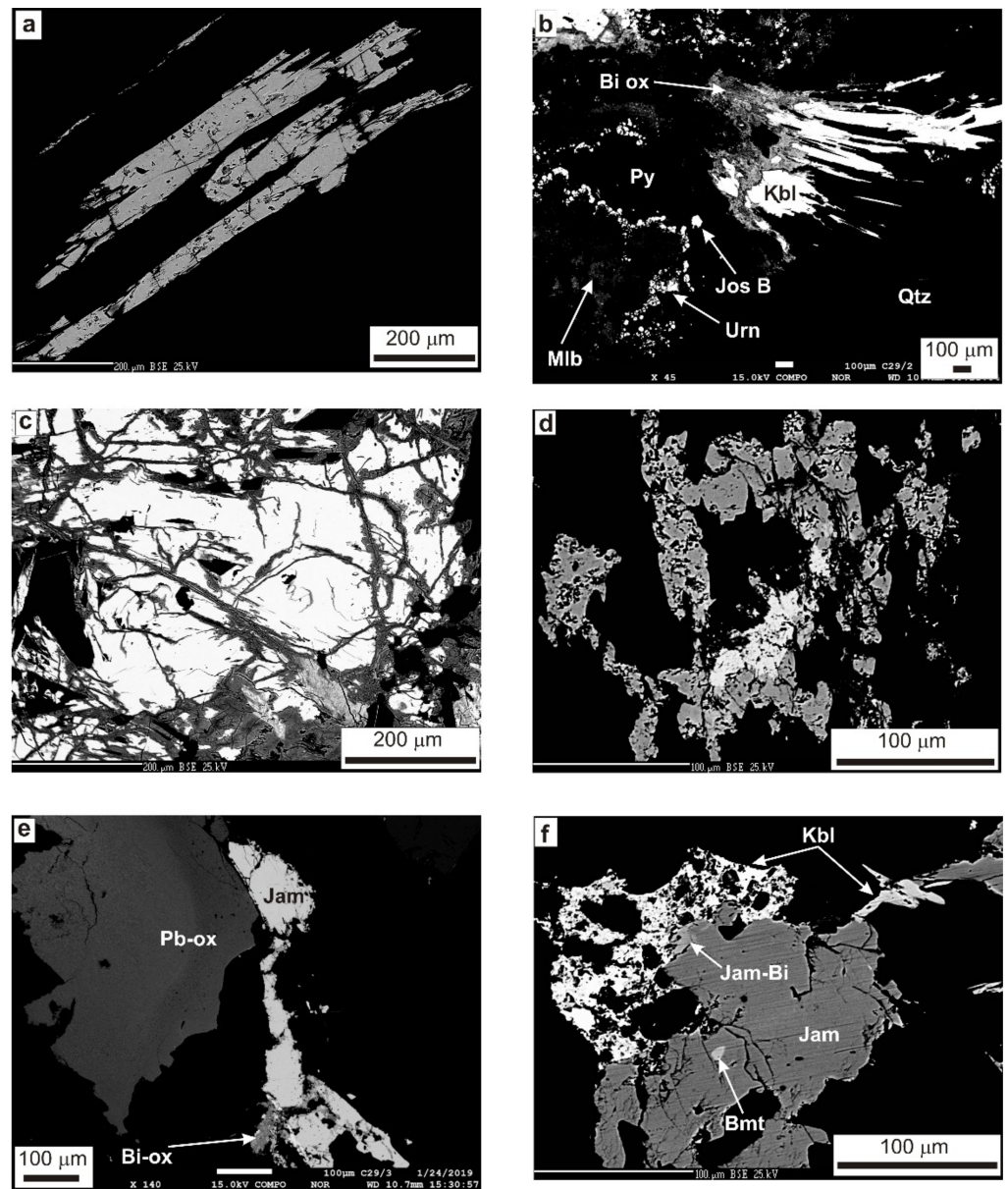
muthinite (type A) grow on needle crystals of minerals of the kobellite–tintinaite series (Figure 7d) or form relicts in a mixture of the supergene minerals, wulfenite and unnamed sulphates of bismuth and lead. The second type of bismuthinite (B) occurs as subhedral grains up to 20  $\mu\text{m}$  in size intergrown with minerals of the kobellite–tintinaite series, jamesonite and galena (Figure 7e), or tiny crystals enclosed in kobellite together with native bismuth (Figure 7f). Bismuthinite A is characterized by a practically zero Sb content and a high content of Bi (with an average of 81.23 wt. %; 2.03 *apfu*), whereas a significant content of Sb (up to 0.54 *apfu*) substituting for Bi is typical for the bismuthinite B. The Bi/(Bi + Sb) ratio in the bismuthinite B is 0.73. The common admixtures in both types of bismuthinite are Pb (up to 1.66 wt. %; 0.04 *apfu*) and Cu (up to 0.49 wt. %; 0.04 *apfu*), and the calculated value of  $n_{\text{aik}}$  [31] is between 0.0 and 3.7. Selenium is practically absent in bismuthinite A (with a maximum of 0.02 wt. %), while bismuthinite B contains up to 0.74 wt. % (0.05 *apfu*) of Se. The chemical composition of bismuthinite A is expressed by the empirical formula,  $(\text{Bi}_{2.03}\text{Pb}_{0.03}\text{Cu}_{0.01})_{\Sigma 2.07}\text{S}_{2.93}$ , and the empirical formula of bismuthinite B is  $(\text{Bi}_{1.45}\text{Sb}_{0.53}\text{Pb}_{0.03}\text{Cu}_{0.03})_{\Sigma 2.04}(\text{S}_{2.92}\text{Se}_{0.04})_{\Sigma 2.96}$ .

**Bismuth** forms anhedral grains up to 10  $\mu\text{m}$  in size, enclosed in minerals of the kobellite–tintinaite series together with bismuthinite (Figure 7f). In addition to the dominant Bi (98.4 wt. %; 0.97 wt. %), only slightly increased contents of Sb (0.01 *apfu*), Cu (0.01 *apfu*), Pb (0.01 *apfu*) and Se (0.01 *apfu*) were found in this mineral phase (Table 9).

**Minerals of the kobellite–tintinaite series** are relatively abundant at the studied occurrence. They form individual acicular crystals up to 1 cm long (Figure 9a) or irregular aggregates up to 2  $\times$  2 cm enclosed in quartz and are always in close proximity to uraninite and molybdenite veinlets. Kobellite–tintinaite mineral phases were found in close association with pyrite, jamesonite, cosalite, sulphotellurides and ullmannite (Figure 9b) as well as minor amounts of galena and native bismuth. Their aggregates are replaced, to various degrees, by oxyplumboroméite (sometimes complete pseudomorphs) and other unspecified oxides of Bi and Pb (Figure 9b,c). The chemical composition of the studied mineral phases (Table 10) is characterized by a wide interval of Bi  $\leftrightarrow$  Sb substitution (Figure 10e), ranging compositionally from kobellite (with Bi, 12.39 *apfu*, Sb, 2.95 *apfu*; Bi/(Bi+Sb) = 0.81) to tintinaite (with Bi, 4.63 *apfu*; Sb, 10.73 *apfu*; Bi/(Bi + Sb) = 0.29). This strong variation is locally causing slightly irregular chemical zoning (Figure 7b). However, most of the studied samples tend to be homogenous and the analyses cluster around the formal boundary between kobellite and tintinaite (Figure 10e).

The calculated value of  $N$  (order number of kobellite homologue [32]) is ranging from 1.81 to 2.00, with an average value of 1.91. The Pb content ranges from 33.76 to 37.23 wt. % (9.75–10.92 *apfu*) and shows a negative correlation with Cu (up to 1.73 wt. %; 1.62 *apfu*; Figure 10b), but a positive correlation with Fe (up to 2.55 wt. %; 2.55 *apfu*; Figure 10c). The overall Cu+Fe content is between 1.90 and 2.68 *apfu* (2.03 *apfu* on average), with Fe negatively correlating with Cu (Figure 10d). Based on the Ag content, the following two groups of minerals of the kobellite–tintinaite series (Figure 10a) can be distinguished: mineral phases with zero Ag content and phases with a slightly increased Ag content (reaching up to 0.24 wt. %; 0.13 *apfu*). In the second case, Ag negatively correlates with Pb. A small amount of Se (up to 0.61 wt. %; 0.46 *apfu*) is always present in the anionic position and it shows a slightly negative correlation with S (Figure 10f).

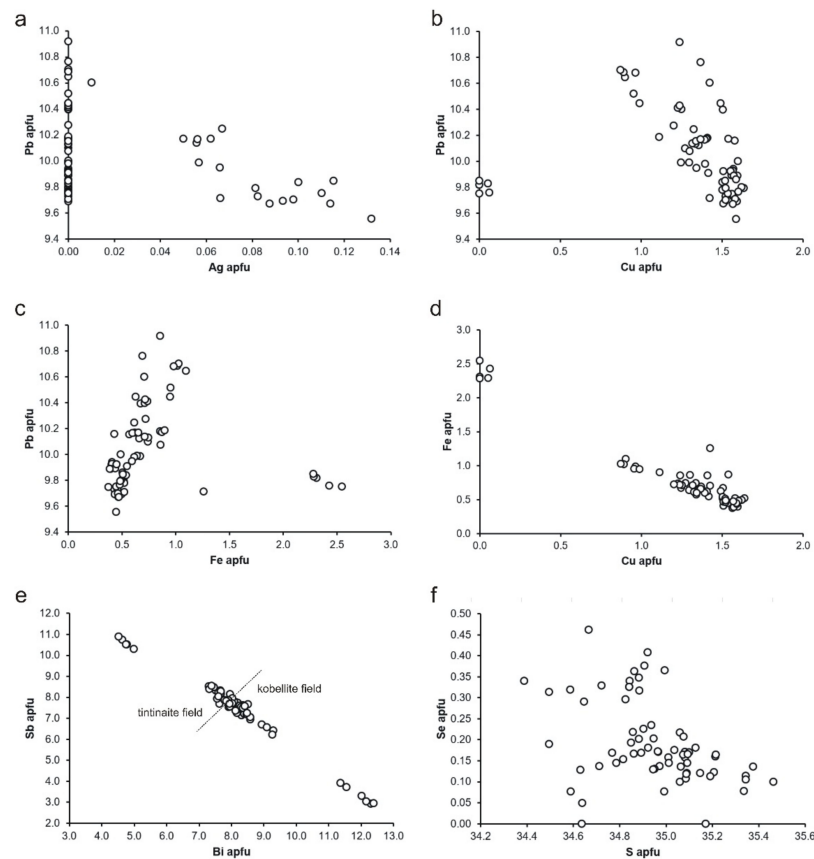
**Cosalite** is an infrequent mineral, and it forms irregular aggregates reaching up to 80  $\mu\text{m}$ , which are closely associated with minerals of the kobellite–tintinaite series and sulphotellurides (Figure 9d). The studied cosalite has a relatively homogeneous chemical composition (Table 11, Figures 11a and 12). The content of Bi fluctuates in the range of 37.55–38.87 wt. % (1.71–1.76 *apfu*). Bismuth is insignificantly substituted by Sb, 3.84–4.52 wt. % (0.30–0.35 *apfu*); the Bi/(Bi + Sb) ratio ranges from 0.83 to 0.86. In the anionic position, S is partially replaced by Se (with a maximum of 1.00 wt. %; 0.12 *apfu*; Figure 11b). Other admixtures (Cd, Cu, Fe) in cosalite are not very important. The content of the above-mentioned elements does not exceed 0.6 wt. % (0.08 *apfu*) for each element separately.



**Figure 9.** (a) Acicular crystals of kobellite–tintinaite series minerals (grey) in quartz (black). (b) Aggregate of needle-like crystals of kobellite–tintinaite series minerals (Kbl) in association with pyrite (Py), joséite-B (Jos B), ullmannite, uraninite (Urn) and molybdenite (Mlb). Kobellite–tintinaite is partially replaced by supergene oxides of Bi-Pb-Sb (Bi ox). The host mineral is quartz (Qtz). (c) Kobellite–tintinaite (white) is replaced by unidentified oxides, Pb-Bi (shades of grey). (d) Cosalite (white) associated with minerals of the kobellite–tintinaite series (grey) in quartz (black). (e) Irregular veinlet of jamesonite (Jam) in quartz (black) is replaced by unspecified supergene minerals of Sb-Pb-Bi (Bi-ox). The cavity in the quartz is filled with supergene oxides of Pb-Fe (Pb-ox). (f) Jamesonite (Jam, Jam-Bi) in contact with kobellite–tintinaite series minerals with enclosed grain of bismuthinite (Bmt). BSE, photos by T. Mikuš (b,e) and M. Števkó (a,c,d,f).

**Table 10.** Representative WDS microanalyses of minerals of the kobellite–tintinaite series from Čučma (Majerská valley).

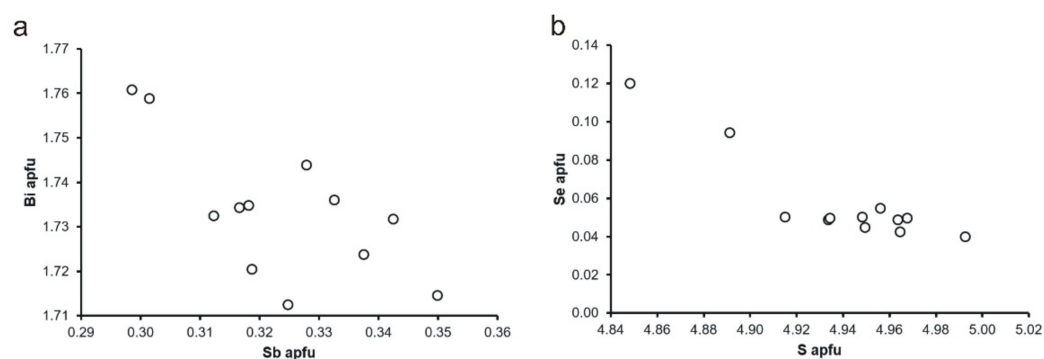
	1	2	3	4	5	6	7	8	9	10	11	12	13	14	15
Ag	0.00	0.00	0.00	0.18	0.24	0.00	0.11		0.02	0.00		0.00	0.00	0.00	0.00
Cu	0.00	0.00	0.00	1.65	1.70	1.30	1.47	1.61	1.51	1.73	1.66	1.29	0.98	0.90	0.89
Fe	2.29	2.29	2.55	0.44	0.42	0.79	0.57	0.38	0.66	0.46	0.35	0.68	0.86	0.96	0.89
Cd	0.00	0.00	0.00	0.31	0.23		0.20			0.09		0.00	0.00	0.00	0.00
Pb	36.70	36.09	36.26	34.28	33.38	37.23	34.70	34.56	36.68	34.12	33.76	35.74	35.20	34.66	34.75
Bi	17.01	17.16	17.91	26.57	27.03	26.24	26.98	28.39	27.64	29.15	29.74	28.28	38.98	40.37	40.63
Sb	23.86	23.18	22.97	17.58	17.00	15.42	15.69	15.96	15.30	15.43	15.62	14.62	7.31	5.61	5.63
S	20.38	20.12	20.33	19.12	18.97	18.25	18.38	18.81	18.46	18.89	18.58	18.61	18.19	17.58	17.54
Se	0.15	0.19	0.11	0.23	0.16	0.10	0.20	0.50	0.41	0.18	0.61	0.23	0.23	0.28	0.27
Total wt. %	100.39	99.03	100.13	100.36	99.13	99.32	98.30	100.21	100.68	100.05	100.32	99.45	101.75	100.36	100.60
Empirical formula (calculated on the basis of 63 atoms)															
Ag	0.000	0.000	0.000	0.098	0.132	0.000	0.062	0.000	0.010	0.000	0.000	0.000	0.000	0.000	0.000
Cu	0.000	0.000	0.000	1.522	1.586	1.239	1.405	1.507	1.423	1.620	1.563	1.225	0.955	0.901	0.892
Fe	2.280	2.311	2.545	0.462	0.446	0.855	0.620	0.405	0.706	0.490	0.375	0.735	0.953	1.094	1.015
Cd	0.000	0.000	0.000	0.162	0.121	0.000	0.108	0.000	0.000	0.048	0.000	0.000	0.000	0.000	0.000
Σ	2.280	2.311	2.545	2.244	2.286	2.094	2.195	1.912	2.139	2.158	1.938	1.960	1.908	1.996	1.908
Pb	9.848	9.818	9.752	9.700	9.554	10.917	10.170	9.924	10.602	9.800	9.747	10.411	10.518	10.647	10.685
Bi	4.526	4.629	4.776	7.454	7.670	7.629	7.840	8.082	7.921	8.301	8.513	8.168	11.548	12.296	12.387
Sb	10.896	10.731	10.513	8.465	8.280	7.693	7.825	7.798	7.528	7.541	7.674	7.247	3.717	2.933	2.946
Σ	15.421	15.360	15.289	15.919	15.950	15.322	15.666	15.881	15.449	15.842	16.187	15.416	15.265	15.229	15.333
S	35.345	35.375	35.337	34.966	35.090	34.589	34.816	34.907	34.496	35.064	34.667	35.037	35.128	34.903	34.857
Se	0.106	0.136	0.078	0.171	0.120	0.077	0.154	0.377	0.314	0.136	0.462	0.176	0.180	0.226	0.218
Σ	35.450	35.511	35.415	35.137	35.210	34.666	34.969	35.283	34.810	35.200	35.129	35.213	35.308	35.128	35.074
Bi/(Sb + Bi)	0.29	0.30	0.31	0.47	0.48	0.50	0.50	0.51	0.51	0.52	0.53	0.53	0.76	0.81	0.81
Sb/(Sb + Bi)	0.71	0.70	0.69	0.53	0.52	0.50	0.50	0.49	0.49	0.48	0.47	0.47	0.24	0.19	0.19



**Figure 10.** Interdependencies of elements in minerals of kobellite–tintinaite series: (a) Ag vs. Pb; (b) Cu vs. Pb; (c) Fe vs. Pb; (d) Cu vs. Fe; (e) Bi vs. Sb; (f) S vs. Se.

**Table 11.** Representative WDS microanalyses of cosalite from Čučma (Majerská valley).

	1	2	3	4	5	6	7	8	9	10
Pb	39.91	39.85	40.50	40.13	40.04	39.75	39.75	40.29	40.06	40.20
Mn	0.08	0.07	0.08	0.09	0.08	0.10	0.08	0.10	0.10	0.07
Fe	0.15	0.13	0.16	0.14	0.15	0.13	0.11	0.15	0.14	0.14
Cu	0.13	0.15	0.18	0.16	0.16	0.51	0.43	0.16	0.18	0.16
Cd	0.44	0.44	0.48	0.50	0.47	0.42	0.39	0.50	0.49	0.49
In	0.06	0.06	0.06	0.08	0.00	0.07	0.00	0.07	0.00	0.07
Sb	4.09	4.07	4.45	4.52	4.15	3.84	3.86	4.15	4.26	4.38
Bi	37.89	38.08	38.62	38.01	37.88	38.87	38.65	37.55	38.16	38.39
S	16.87	16.73	16.88	16.83	16.38	16.42	16.49	16.65	16.64	16.96
Se	0.33	0.41	0.41	0.42	0.41	1.00	0.78	0.37	0.41	0.41
Total wt. %	99.95	99.99	101.82	100.88	99.72	101.11	100.54	99.99	100.44	101.27
Empirical formula (calculated on the basis of 9 atoms)										
Pb	1.828	1.831	1.832	1.826	1.859	1.816	1.824	1.853	1.838	1.820
Mn	0.014	0.012	0.014	0.015	0.014	0.017	0.014	0.017	0.017	0.012
Fe	0.025	0.022	0.027	0.024	0.026	0.022	0.019	0.026	0.024	0.024
Cu	0.019	0.022	0.027	0.024	0.024	0.076	0.064	0.024	0.027	0.024
Cd	0.037	0.037	0.040	0.042	0.040	0.035	0.033	0.042	0.041	0.041
In	0.005	0.005	0.005	0.007	0.000	0.006	0.000	0.006	0.000	0.006
Σ	1.928	1.930	1.944	1.937	1.963	1.972	1.954	1.968	1.948	1.926
Sb	0.319	0.318	0.342	0.350	0.328	0.299	0.301	0.325	0.333	0.338
Bi	1.720	1.735	1.732	1.715	1.744	1.761	1.759	1.712	1.736	1.724
Σ	2.039	2.053	2.074	2.064	2.072	2.059	2.060	2.037	2.069	2.061
S	4.993	4.968	4.934	4.948	4.915	4.848	4.891	4.950	4.934	4.964
Se	0.040	0.049	0.049	0.050	0.050	0.120	0.094	0.045	0.049	0.049
Σ	5.032	5.017	4.982	4.999	4.965	4.968	4.985	4.994	4.984	5.013
Bi/(Bi+Sb)	0.84	0.84	0.83	0.83	0.84	0.86	0.85	0.84	0.84	0.84

**Figure 11.** Interdependence of Sb vs. Bi (a) and S vs. Se (b) in cosalite from Čučma (Majerská valley).

*Jamesonite* forms irregular veinlets (with a length of up to 1 mm) in quartz (Figure 9e) or subhedral grains and aggregates up to 150  $\mu\text{m}$  that are intimately intergrown with minerals of the kobellite–tintinaite series (Figure 9f). Supergene Fe–Pb–Bi oxides fill the fissures in the jamesonite or replace it. In terms of chemical composition, the studied jamesonite is interesting mainly due to the relatively stable admixture of Bi (with an average of 16.48 wt. %; 1.77 *apfu*; Table 12). Rarely, the Bi content reaches up to 24.23 wt. % (2.67 *apfu*) and it causes slight chemical zoning (Figure 9f). The Sb content averages around 23.45 wt. % (4.32 *apfu*), and in Bi-rich jamesonite the Sb content decreases to 17.87 wt. % (3.38 *apfu*). Weakly increased contents of Cu (up to 0.15 wt. %; 0.05 *apfu*), As (up to 0.13 wt. %; 0.04 *apfu*) and Se (with a maximum of 0.40 wt. %; 0.12 *apfu*) were also

detected. The chemical composition of the studied jamesonite corresponds to the following empirical formulae:

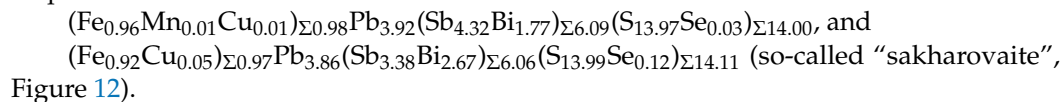


**Table 12.** Chemical composition of jamesonite from Čučma (Majerská valley).

	1	2	3	4	5	6	7	8	9	10	11
Fe	2.38	2.40	2.36	2.37	2.39	2.62	2.46	2.29	2.32	2.23	0.48
Mn			0.05	0.00	0.07	0.05	0.06	0.05	0.05	0.00	0
Cu			0.00	0.00	0.00	0.08	0.07	0.00	0.00	0.15	1.55
Pb	36.70	36.70	36.14	35.69	36.12	36.33	36.56	36.43	35.70	34.72	33.47
As	0.02	0.13									
Sb	23.48	23.33	23.15	23.53	23.58	23.56	23.68	23.67	23.08	17.87	16.14
Bi	16.15	16.28	16.68	16.37	16.70	16.61	16.37	16.44	16.69	24.23	27.59
S	19.52	19.39	20.11	20.21	20.42	20.27	20.05	19.93	20.10	19.45	18.81
Se			0.17	0.15	0.15	0.14	0.19	0.17	0.14	0.40	0.24
Total wt. %	98.25	98.22	98.66	98.32	99.43	99.66	99.44	98.98	98.08	99.05	98.28
Empirical formula (calculated on the basis of 25 atoms)											
Fe	0.970	0.979	0.946	0.949	0.946	1.037	0.980	0.920	0.933	0.921	0.205
Mn			0.020	0.000	0.028	0.020	0.024	0.020	0.020	0.000	0.000
Cu			0.000	0.000	0.000	0.028	0.025	0.000	0.000	0.054	0.581
Σ	0.970	0.979	0.966	0.949	0.974	1.085	1.029	0.940	0.954	0.975	0.786
Pb	4.029	4.040	3.904	3.850	3.854	3.874	3.927	3.944	3.870	3.863	3.850
As	0.006	0.038									
Sb	4.387	4.371	4.256	4.319	4.281	4.275	4.328	4.360	4.258	3.384	3.160
Bi	1.758	1.777	1.786	1.751	1.767	1.756	1.743	1.764	1.794	2.673	3.147
Σ	6.152	6.186	6.042	6.070	6.048	6.032	6.072	6.125	6.052	6.057	6.306
S	13.848	13.796	14.040	14.089	14.081	13.970	13.919	13.943	14.084	13.988	13.985
Se			0.048	0.042	0.042	0.039	0.054	0.048	0.040	0.117	0.072
Σ	13.848	13.796	14.088	14.132	14.123	14.009	13.972	13.992	14.124	14.104	14.057
Sb/(Sb+Bi)	0.71	0.71	0.70	0.71	0.71	0.71	0.71	0.71	0.70	0.56	0.50

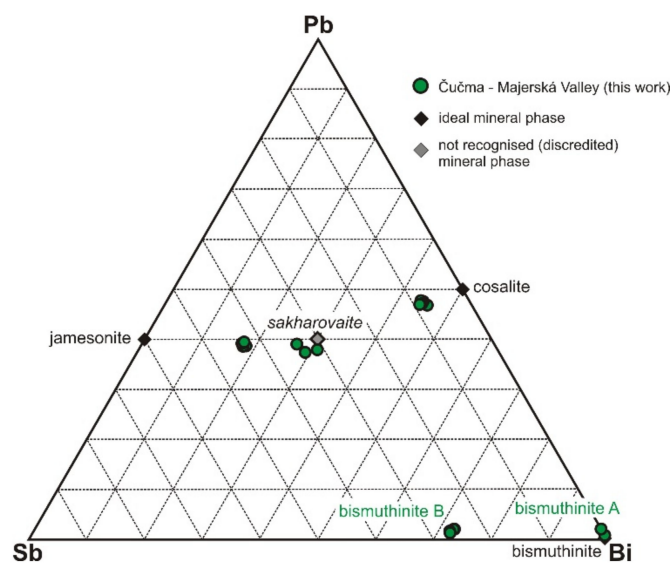


**Figure 12.** Chemical composition of bismuthinite, Sb-bearing cosalite and Bi-bearing jamesonite from Čučma, in ternary system Sb-Bi-Pb.

**Galena** occurs as subhedral grains up to 20  $\mu\text{m}$  in size or aggregates intimately intergrown with bismuthinite and minerals of the kobeinite–tintinaite series (Figure 7e). The chemical composition of galena is given in Table 13. From the admixtures, Bi (up to 0.01 *apfu*) and Se (up to 0.07 *apfu*) are relatively important, while the content of other elements is insignificant. The average empirical formula of the studied galena is  $(\text{Pb}_{0.97}\text{Bi}_{0.01})_{\Sigma 0.98}(\text{S}_{0.96}\text{Se}_{0.07})_{\Sigma 1.03}$ .

**Table 13.** Chemical composition of galena from Čučma (Majerská valley).

	1	2
Pb	83.76	83.41
Fe	0.00	0.05
Cu	0.09	0.06
In	0.06	0.06
Bi	0.70	0.57
S	12.81	12.79
Se	2.11	2.32
Total wt. %	99.55	99.27
Empirical formula (on 2 atoms)		
Pb	0.967	0.963
Fe	0.000	0.002
Cu	0.004	0.002
In	0.001	0.001
Bi	0.008	0.007
$\Sigma$	0.980	0.975
S	0.956	0.954
Se	0.064	0.070
$\Sigma$	1.020	1.025

#### 4.2.2. Non-Ore and Accessory Minerals

**Quartz** is a dominant component of the gangue. In the transmitted light, the two generations of quartz were identified. Quartz I forms weakly undulous, anhedral grains (up to 5 mm in size), embedded in quartz II. Edges of these grains are partially melted and recrystallized. Quartz II is an essential part of the gangue. It is fine-grained, the size of individual anhedral grains is around 0.1–0.2 mm. The undulosity was not observed. Ore minerals are accumulated mainly at the interfaces of quartz I and II aggregates but penetrate both quartz generations.

**Fluorapatite** is a typical and the most wide-spread accessory mineral of the gangue. It forms subhedral crystals (with square cross-sections), or anhedral grains up to 0.5 mm in size, irregularly scattered in both generations of quartz or in close spatial association with U-Mo minerals (Figures 4d and 13a). Therefore, this position probably indicates at least two generations of fluorapatite. Locally, fluorapatite is overgrown with aggregates of uraninite, and cracks or cavities in fluorapatite are filled with supergene uranyl minerals (Figure 13b). Fluorapatite from the Majerská valley is generally characterized by an overall low content of admixtures and, besides Ca and P (Table 14), only minor amounts of Y and REE are present. The average content of  $\text{Y}_2\text{O}_3 + \text{REE}_2\text{O}_3$  in fluorapatite is 0.51 wt. % (0.02 *apfu*; Y + REE). Except of Y, LREE (0.28 wt. %  $\text{LREE}_2\text{O}_3$ ; 0.01 *apfu* LREE) slightly predominates over HREE (0.15 wt. %  $\text{HREE}_2\text{O}_3$ ; 0.004 *apfu* HREE). The hydroxyl groups  $(\text{OH})^-$  are locally indistinctly present (reaching up to 0.08 *apfu*), at the expense of the reduced F content. The average empirical formula of studied fluorapatite is  $(\text{Ca}_{4.92}\text{Y} + \text{REE}_{0.02})_{\Sigma 4.94}(\text{PO}_4)_{3.01}(\text{F}_{1.01}\text{OH}_{0.03})_{\Sigma 1.04}$ .

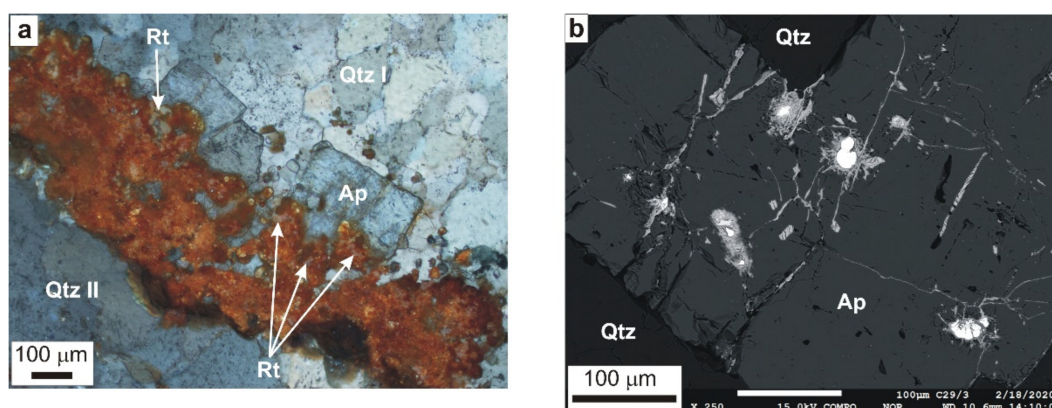


**Figure 13.** (a) Subhedral crystals of fluorapatite (Ap) in quartz (Qtz), replaced by unspecified supergene U mineral (orange–brown), which represent complete pseudomorphosis after the original uraninite veinlet. Small grains of rutile (Rt) are also enclosed by supergene U mineral. (b) Small cavities and cracks in fluorapatite (Ap) are filled with uraninite (white) and supergene uranyl minerals (light grey). The host mineral is quartz (Qtz). Picture a—transmitted light, PPL (photo: Š. Ferenc), picture b—BSE (photo: T. Mikuš).

**Zircon** was found mainly in quartz II. It forms thin, long prismatic crystals with lengths of up to 50  $\mu\text{m}$ . Aggregates of flaky crystals of unspecified *chlorites* fill thin fissures or small cavities in the quartz. Chlorite aggregates are also developed in interstitial spaces between ore minerals (uraninite, molybdenite, tetradymite; Figure 7a). Small veinlets of *titanite* rarely cut molybdenite veins, enclosing aggregates of molybdenite crystals (Figure 7a). *Rutile* forms irregular grains (up to 50  $\mu\text{m}$  in size), enclosed in uraninite and molybdenite, respectively, by supergene uranyl minerals (Figure 13a). *Minerals of the tourmaline group (schorl to dravite)* occur as individual acicular crystals up to 3 mm or as irregular nests up to 1.5 cm in size enclosed in quartz.

**Table 14.** Representative WDS microanalyses of fluorapatite from Čučma (Majerská valley).

	1	2	3	4	5	6
Na <sub>2</sub> O	0.04	0.03	0.03	0.04	0.01	0.03
CaO	55.03	55.15	55.17	55.47	55.33	55.49
BaO	0.29	0.00	0.00	0.12	0.00	0.00
MnO	0.01	0.00	0.04	0.00	0.00	0.04
FeO	0.00	0.00	0.02	0.10	0.04	0.01
PbO	0.00	0.00	0.00	0.01	0.00	0.02
Al <sub>2</sub> O <sub>3</sub>	0.02	0.00	0.00	0.01	0.00	0.00
Y <sub>2</sub> O <sub>3</sub>	0.08	0.08	0.08	0.01	0.13	0.09
La <sub>2</sub> O <sub>3</sub>	0.05	0.00	0.03	0.01	0.06	0.00
Ce <sub>2</sub> O <sub>3</sub>	0.04	0.06	0.08	0.07	0.09	0.08
Pr <sub>2</sub> O <sub>3</sub>	0.01	0.01	0.10	0.00	0.00	0.06
Nd <sub>2</sub> O <sub>3</sub>	0.03	0.05	0.06	0.06	0.05	0.12
Sm <sub>2</sub> O <sub>3</sub>	0.02	0.00	0.00	0.07	0.12	0.03
Eu <sub>2</sub> O <sub>3</sub>	0.00	0.02	0.04	0.00	0.01	0.04
Gd <sub>2</sub> O <sub>3</sub>	0.10	0.08	0.04	0.04	0.01	0.00
Tb <sub>2</sub> O <sub>3</sub>	0.01	0.02	0.00	0.02	0.00	0.06
Dy <sub>2</sub> O <sub>3</sub>	0.08	0.00	0.00	0.00	0.12	0.03
Ho <sub>2</sub> O <sub>3</sub>	0.10	0.04	0.01	0.04	0.12	0.00
Er <sub>2</sub> O <sub>3</sub>	0.02	0.02	0.00	0.00	0.08	0.00
Lu <sub>2</sub> O <sub>3</sub>	0.00	0.00	0.04	0.02	0.09	0.00
TiO <sub>2</sub>	0.06	0.00	0.09	0.01	0.09	0.11
ZrO <sub>2</sub>	0.06	0.11	0.05	0.06	0.10	0.11
ThO <sub>2</sub>	0.01	0.00	0.00	0.01	0.00	0.00
UO <sub>2</sub>	0.00	0.02	0.02	0.00	0.00	0.01
SiO <sub>2</sub>	0.04	0.03	0.00	0.01	0.00	0.01
P <sub>2</sub> O <sub>5</sub>	42.82	43.00	42.42	43.06	42.63	42.88

Table 14. Cont.

	1	2	3	4	5	6
As <sub>2</sub> O <sub>5</sub>	0.01	0.10	0.02	0.00	0.03	0.00
SO <sub>3</sub>	0.01	0.02	0.00	0.03	0.02	0.01
H <sub>2</sub> O *				0.31	0.27	0.04
F	4.21	4.20	3.89	3.47	3.50	3.77
Total wt. %	103.15	103.01	102.23	103.03	102.86	103.03
F = O	−1.77	−1.77	−1.64	−1.46	−1.47	−1.59
Total wt. %	101.37	101.25	100.59	101.57	101.39	101.45
Empirical formula (calculated on the basis of 13 anions)						
Na	0.006	0.005	0.004	0.006	0.002	0.004
Ca	4.882	4.883	4.937	4.934	4.945	4.928
Ba	0.009	0.000	0.000	0.004	0.000	0.000
Mn	0.001	0.000	0.003	0.000	0.000	0.003
Fe	0.000	0.000	0.002	0.007	0.003	0.000
Pb	0.000	0.000	0.000	0.000	0.000	0.000
Al	0.002	0.000	0.000	0.001	0.000	0.000
Y	0.004	0.004	0.004	0.000	0.006	0.004
La	0.002	0.000	0.001	0.000	0.002	0.000
Ce	0.001	0.002	0.002	0.002	0.003	0.002
Pr	0.000	0.000	0.003	0.000	0.000	0.002
Nd	0.001	0.001	0.002	0.002	0.001	0.004
Sm	0.001	0.000	0.000	0.002	0.003	0.001
Eu	0.000	0.001	0.001	0.000	0.000	0.001
Gd	0.003	0.002	0.001	0.001	0.000	0.000
Tb	0.000	0.001	0.000	0.000	0.000	0.002
Dy	0.002	0.000	0.000	0.000	0.003	0.001
Ho	0.003	0.001	0.000	0.001	0.003	0.000
Er	0.001	0.000	0.000	0.000	0.002	0.000
Lu	0.000	0.000	0.001	0.001	0.002	0.000
Ti	0.004	0.000	0.006	0.001	0.006	0.007
Zr	0.003	0.005	0.002	0.002	0.004	0.004
Th	0.000	0.000	0.000	0.000	0.000	0.000
U	0.000	0.000	0.000	0.000	0.000	0.000
Σ M	4.923	4.904	4.970	4.964	4.985	4.964
Si	0.003	0.002	0.000	0.001	0.000	0.001
P	3.001	3.008	3.000	3.027	3.010	3.009
As	0.000	0.004	0.001	0.000	0.001	0.000
S	0.001	0.001	0.000	0.002	0.001	0.001
Σ T	3.006	3.016	3.001	3.030	3.012	3.010
F	1.102	1.098	1.028	0.911	0.923	0.988
OH				0.089	0.077	0.012
Σ X	1.102	1.098	1.028	1.000	1.000	1.000

\* H<sub>2</sub>O content is calculated based on the number of OH in empirical formula.

## 5. Discussion

### 5.1. Succession of Mineralization

The microstructural relationships of vein filling minerals suggest that the studied mineralization originated, most probably, in the following stages:

- (I.) quartz I, fluorapatite I;
- (II.) quartz II, fluorapatite II, zircon, rutile chlorite, tourmaline;
- (III.) uraninite, molybdenite, U-Ti oxides;
- (IV.) (?) pyrite I (non-zonal), ullmannite, gersdorffite, cobaltite;
- (Va.) (?) galena, bismuth, tetradymite, joséite A and B, Bi<sub>3</sub>(TeS)<sub>2</sub> mineral phase, (BiPb)(TeS) mineral phase, ikonolite;
- (Vb.) kobellite–tintinaite series mineral phases, cosalite;

- (VI.) pyrite II (zonal);
- (VII.) titanite, chlorite;
- (VIII.) supergene mineral phases.

Similarly, Varček [5] states that U-REE mineralization in quartz-fluorapatite veins near Čučma (Gemic Unit) is accompanied by younger quartz, Fe and Fe-Mg carbonates and a diverse range of sulphidic minerals.

## 5.2. Mineralization Type

In the Gemic Unit, quartz and quartz-apatite veins with U and U-REE mineralization and accompanying Au and sulphidic mineralization are widespread in several localities, including the following: Hnilec-Peklisko, Gemerská Poloma-Krátka valley [5,7,33,34], Henclová [4], Čučma-Kutačka vein and other occurrences [1,5,6,8–10,33,34], Betliar [6,9], Prakovce-Zimná voda [7,34–37] and Zlatá Idka [2,6]. Their common feature is the location of the Lower Paleozoic rocks in the vicinity of the intrusions of the Permian Gemic granites.

According to our own, as well as previous, mineralogical research by Varček [5] or Rojkovič [9], it is possible to divide uranium (and REE)-bearing quartz ( $\pm$ apatite) veins into the following two main types (based on the association of main primary minerals and the content of P and Y + REE):

**(A) Hydrothermal quartz-apatite veins containing U-REE mineralization** (Betliar, Čučma-Kutačka vein, and some veins in the Majerská valley area) are characterized by a high content of P (0.11–3.47 wt. %) and Y + REE (up to 1.23 wt. %). Although Varček [5] reports a rich association of sulphide minerals from the Kutačka vein, this type of mineralization is characterized by a very low to zero sulphide content, as evidenced by the overall low S content (<0.04 wt. %; quartz-apatite vein with U-REE mineralization from the Majerská valley; Table 1). Besides quartz and apatite, major primary minerals are represented by Y- and REE-bearing minerals (such as monazite-(Ce) to monazite-(Nd) and xenotime-(Y)), uraninite, rutile and titanite [5,6,8–10,33,34]. The element association typical of this mineralization type is Si-P-Ca-U-REE. Rojkovič et al. [9] also mentioned increased contents of Pb, Mo and Au. Despite the increased Mo content, molybdenite is a rare mineral in microscopic amounts. From other sulphides, pyrite is relatively abundant, and galena was found only as a minor mineral phase (Števko, unpublished data).

**(B) Hydrothermal quartz veins (with no or minor apatite content) containing U-( $\pm$ sulphidic)-( $\pm$ Au)-( $\pm$ REE) mineralization** (Hnilec-Peklisko, Gemerská Poloma-Krátka valley, Henclová, Prakovce-Zimná voda and Zlatá Idka). This type of mineralization is characterized by a zero to very low (up to 0.1 wt. %) content of P. The Y + REE content is generally also reduced, compared to the first type of mineralization; their significantly increased content (with an average of 0.17 wt. %) was found only in the Zimná voda locality. Apatite and Y and REE-bearing phases are only accessory minerals. The content of sulphides in this type of mineralization is variable but stable. Besides quartz, the essential primary minerals are represented by uraninite, brannerite (in different quantitative ratios) and rutile, accompanied by tourmaline and rich assemblage of the following sulphidic minerals: Fe-Ni-Co sulphoarsenides, pyrite, chalcopyrite, galena, tetrahedrite, gold, bismuthinite, millerite, sphalerite, pyrrotite, etc. Molybdenite is very rare in this mineralization type. The typical element association is Si-(P)-(Ca)-U-Ni-Co-Fe-Pb-Bi-Au-Ti-Zr-B.

The studied quartz veins containing U-Mo mineralization from the Majerská valley can be included in the first approximation to the above-mentioned mineralization type B. However, it is necessary to note some of their peculiarities, as follows:

- Compared to type A, fluorapatite is only a minor component in the studied veins (it only has the character of an accessory mineral), as evidenced by the XRF map of Ca and P distribution in the gangue (Figure 3) and a significantly reduced content of those elements (see Table 1).
- The most abundant ore minerals are molybdenite and uraninite, accompanied by a diverse (but less represented) assemblage of sulphides (pyrite, galena), sulphos-

alts (mainly minerals of the kobellite–tintinaite series), sulphoarsenides (cobaltite, gersdorffite, ullmannite), Bi minerals (bismuth, bismuthinite) and sulphotellurides (tetradymite, joséite-A, joséite-B, etc.).

- The typical association of the elements in the studied veins is (the elements in parentheses have a less significance) as follows: Si-(P)-(Ca)-U-Mo-(Pb)-(Bi)-(Te).

Therefore, the significantly reduced P content and the abundant presence of sulphidic minerals allow for the classification of the studied veins into the mineralization type B. However, they notably differ from this type of mineralization by the abundant presence of molybdenite as well as an elevated content of Te. In the vein U-(REE) mineralization hosted in the Lower Paleozoic rocks of the Gemeric Unit, molybdenite was only rarely found at the Zimná voda locality [36] and Čučma-Kutačka (Števkó, unpublished data). In the Gemeric Unit, an abundance of molybdenite, besides uraninite, is a characteristic feature of deposits and occurrences of stratiform, veinlets and stockwork, mainly volcanogenic (or tectonic) U-Mo mineralization hosted in Upper Paleozoic (Permian) rocks of Northern Gemeric (e.g., Novoveská Huta, Košice-Kurišková, Košická Hámre, Matejovce nad Hornádom; [33,34,38]). In general, acidic to intermediate volcanic effusive rocks and their pyroclastics represent a significant source of U and Mo for this type of mineralization [39,40]. The most important and widespread volcanogenic mineralization in the world is associated with felsic, acidic volcanics—rhyolites, e.g., McDermitt and Virgin Valley caldera deposits in the USA [41], Ben Lomond and Maureen deposits in Australia [42,43], or Smolian deposit in Bulgaria [44].

On this basis, the studied quartz veins with U-Mo mineralization in Majerská valley near Čučma can be defined as a separate subtype of the above-mentioned hydrothermal vein mineralization of type B.

### 5.3. Genesis and Age of U-Mo Mineralization

Quartz and quartz-apatite veins containing U and U-REE mineralization are relatively widespread in the Gemeric Unit; however, their exact dating is still scattered. In addition, there are two fundamentally different views on the genesis of this type of hydrothermal mineralization. Rojkovič [34] and Rojkovič et al. [9,36,45] considered mineralization as Hercynian (although without any dating), whereby the Permian Gemeric granites presumably provided fluids and thermal energy. The hydrothermal effect of granites could have caused a mobilization of P, REE and U from the surrounding Lower Paleozoic graphitic phyllites, metalydites and metaphosphates, and a subsequent concentration of these elements in the hydrothermal veins. However, these authors also admit the possible younger, Alpine age of mineralization. On the contrary, the recent electron-microprobe U–Pb uraninite dating from Čučma [10] gave a Palealpine age ( $207 \pm 2$  Ma; Late Triassic). On this basis, Permian granites are still considered as a possible source of mineralization elements. However, mobilization of P, F, U, REE and Y from granites and their concentration in the hydrothermal veins had to occur during the Late Triassic tectonothermal rejuvenation of the Gemeric Unit [46].

Questions regarding the petrology, geochemistry and age of the Gemeric granites have been solved by several authors. The granitic rocks of the Gemeric Unit represent a distinct type of specialized (Sn–W–F), highly evolved suite with S-type affinity that differs from other granitoids occurring in the Veporic and Tatric Units of the Western Carpathian crystalline basement. They are enriched in fluorine, phosphorus and rare lithophile elements, such as Li, Rb, Cs, B, Ga, Sn, W, Nb, Ta and U (e.g., [23,47–51] and others). More recent zircon U–Pb and molybdenite Re–Os isotopic dating, as well as the chemical ages of monazite, indicate emplacement of the Gemeric granites and related post-magmatic mineralization during Late Permian period. More specifically, the age of the Hnilec granites (in the tectonic zone so-called Northern Gemeric hotline) ranges from 289 to 238 Ma (with an average of 262 Ma) [46,51–54]. The age of the granites emplaced in the Southern Gemeric hotline (Betliar, Elisabeth Mine, Zlatá Idka and Poproč bodies) varies between 303 and 241 Ma (with an average of 266 Ma) [46,51,53].

In the Čučma area, granitic rocks do not reach the surface. The Čučma granite was uncovered by mining works on the Gabriela quartz-stibnite vein, and it was also drilled by borehole Sb-3, 700 m to the NE of the studied locality, at a depth of about 330 m below the surface [55].

The chemical in situ electron-microprobe U-Pb dating of uraninite (Table 3) from the studied U-Mo mineralization hosted in a hydrothermal quartz vein, yielded an average age of 265 Ma, corresponding to the Guadalupian Epoch of Permian. The data obtained corresponds very well with the age of the Gemic granites, especially with the age of the nearby Betliar granite intrusion (268–264 Ma; [51]), outcropping less than 3 km to the NW of the studied locality. The hidden body of the Čučma granite is less than 1 km (400–800 m) away from the studied vein. In frame of hydrothermal mineralizations, the age of the studied uraninite (Majerská valley) agrees with the age of molybdenite of pneumatolytic (greisen type) Sn-Mo mineralization (263 ± 0.9 Ma; [54]), directly genetically related to the Hnilec granite body (Figure 14).

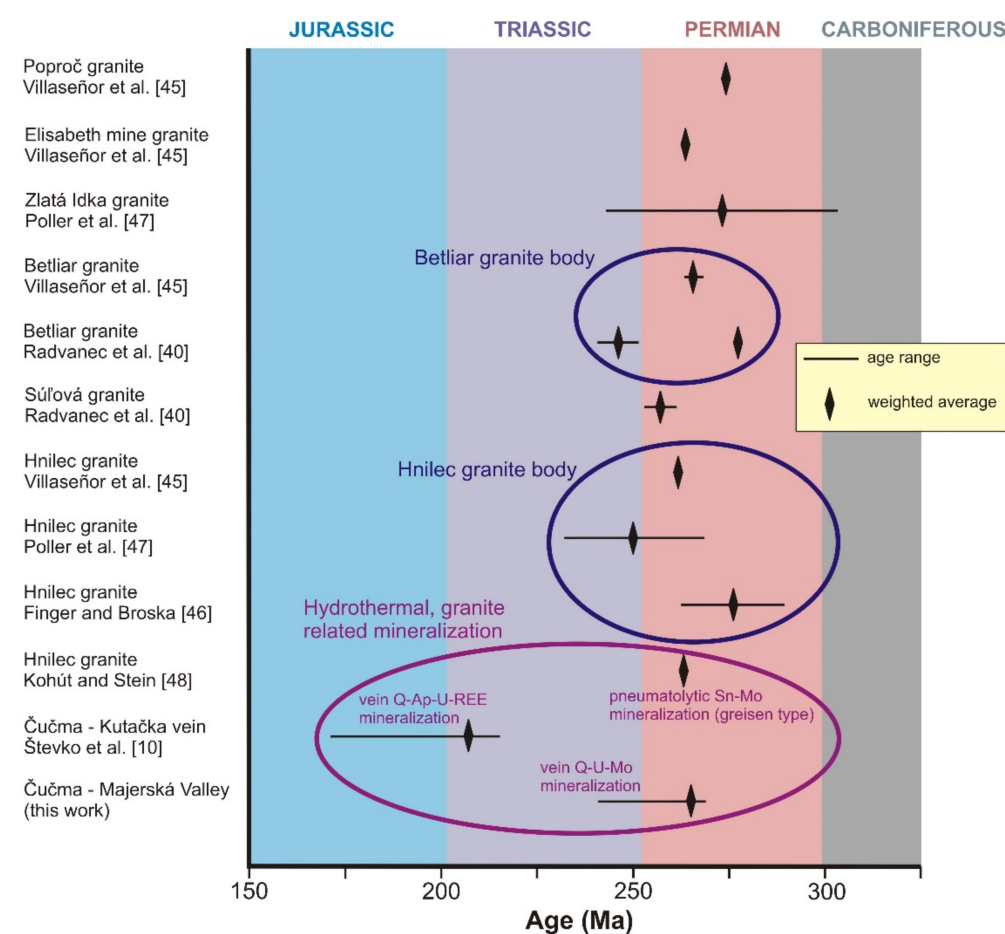


**Figure 14.** Summary of the age data of the Gemic granites and associated hydrothermal mineralization. The age boundaries of the stratigraphic periods are plotted according to the ICS [56].

The dating of studied uraninite clearly confirmed its Hercynian age. The correlation of its age with published data about the age of the Gemic granites [46,51–54] as well as the spatial connection of the studied mineralization with the Čučma granite is clearly pointing to a direct connection between post-collisional S-type granites and the studied U-Mo mineralization. This supports the view of Rojkovič [34] and Rojkovič et al. [9,36,45], that the Gemic granites were donors of fluids, thermal energy and elements such as P, REE, U, etc. In addition, some fluids were mobilized via a hydrothermal effect of granites from the surrounding Lower Paleozoic metasediments. A number of published works have shown that uraninite is sensitive to subsequent post-mineralization processes (e.g., [57–63]),

which are also reflected in the results of dating. From this point of view, the younger age of uraninite obtained from the U-REE-bearing quartz-fluorapatite vein at Čučma by Števko et al. [10] (Figure 14) reflect subsequent, Palealpine processes and might represent a younger, remobilized generation of uraninite, although the whole mineralization is also originally related to S-type granitic magmatism. Such remobilization of Hercynian, hydrothermal vein U mineralization in the Gemeric Unit is also supported by the dual, Hercynian and Alpine ages acquired by the chemical dating of uraninite from the Zlatá Idka and Prakovce-Zimná voda occurrences (Ondrejka—unpublished data, Ferenc and Kopáček—unpublished data).

The classification of the vein uranium deposits (summary in [64]) is based on the presence or absence of other mineral components besides U minerals, also on their geological setting. According to these classifications [65–68], the studied quartz veins with U-Mo and accompanying sulphidic mineralization at the Majerská Valley near Čučma can be qualified as a granite-related (perigranitic) with a complex mineral association (although the representation of other minerals, except uraninite and molybdenite, is inferior).

## 6. Conclusions

Quartz and quartz-apatite veins containing U and U-REE mineralization and the accompanying Au and sulphidic mineralization are widespread at several localities, hosted in Lower Paleozoic rocks of the Gemeric Unit. Ore mineralization at the studied hydrothermal quartz vein at the Majerská valley near Čučma is mainly represented by uraninite and molybdenite, accompanied by a diverse association of sulphides, sulphosalts and sulphotellurides. The chemical in-situ electron-microprobe U-Pb dating of uraninite from the hydrothermal veins yielded an average age of 265 Ma, corresponding to the Guadalupian Epoch of Permian; the obtained data correspond with the age of the Gemeric S-type granites, and also with the age of the greisen type Sn-Mo mineralization associated with them. The age correlation of uraninite with Gemeric granites and the spatial connection of the studied mineralization with the Čučma granite allows us to assume that it is a Hercynian, granite-related (perigranitic) mineralization.

**Author Contributions:** Conceptualization, Š.F. and M.Š.; methodology, T.M. and S.M.; software, R.K. and E.H.; investigation, Š.F. and M.Š.; data curation, Š.F.; writing—original draft preparation, Š.F.; writing—review and editing, M.Š. and Š.F. All authors have read and agreed to the published version of the manuscript.

**Funding:** The SLOVAK RESEARCH AND DEVELOPMENT AGENCY under the contract APVV-19-0065, as well as the MINISTRY OF EDUCATION, SLOVAK REPUBLIC VEGA-1/0237/18 and KEGA 033UMB-42021 projects funded this research.

**Data Availability Statement:** The data presented in this study are available on request from the corresponding author. The data are not publicly available because all representative data are contained in this work.

**Acknowledgments:** The authors thank to Patrik Konečný from the State Geological Institute of D. Štúr (Bratislava) for precise dating microprobe analyses of uraninite and reviewers for their precise reviews and improvement of the manuscript.

**Conflicts of Interest:** The authors declare no conflict of interest. The funders had no role in the design of the study; in the collection, analyses, or interpretation of data; in the writing of the manuscript, or in the decision to publish the results.

## References

1. Šváb, J.; Tulis, J.; Badár, J. *Final Report about Results of Geological Survey in Čučma Locality*; State Geological Institute of D. Štúr Archive: Bratislava, Slovakia, 1966. (In Slovak)
2. Melnikova, A.M. *Short Reports of Mineral Composition of Some Uranium Occurrences in Slovakia*; Uranpres Archive: Spišská Nová Ves, Slovakia, 1973. (In Russian)
3. Tréger, M. Occurrences of uranium-bearing phosphates in the Spišsko-gemerské rudohorie Mts. *Miner. Slov.* **1973**, *5*, 61–64. (In Slovak)

4. Varček, C. *Mineralogical Research of Vein Uranium Mineralization in the Central Part of the Spišsko-Gemerské Rudohorie Mts*; Uranpres Archive: Spišská Nová Ves, Slovakia, 1975. (In Slovak)
5. Varček, C. Some rare types of mineralization in the Spišsko-gemerské rudohorie Mts. In *Deposit Forming Processes in the Western Carpathians Conference Proceedings, Bratislava, Slovakia, 29–30 May 2019*; Háber, M., Ed.; FNS UK: Bratislava, Slovakia, 1977; pp. 93–99.
6. Donát, A. *Evaluation of REE Anomalies Occurrences in the Permian and in the Gelnica Group of SGRI*; State Geological Institute of D. Štúr Archive: Bratislava, Slovakia, 1998. (In Slovak)
7. Donát, A.; Mihál, F.; Novotný, L. *Geological Survey Works on Au in the Older Paleozoic in SGR*; State Geological Institute of D. Štúr Archive: Bratislava, Slovakia, 2000. (In Slovak)
8. Rojkovič, I. Minerals of the crandallite series in quartz-apatite vein near Čučma. *Miner. Slov.* **1993**, *25*, 151–153. (In Slovak)
9. Rojkovič, I.; Konečný, P.; Novotný, L.; Puškelová, L.; Streško, V. Quartz-apatite-REE vein mineralization in Early Paleozoic rocks of the Gemeric Superunit, Slovakia. *Geol. Carpath.* **1999**, *50*, 215–227.
10. Števko, M.; Uher, P.; Ondrejka, M.; Ozdín, D.; Bačík, P. Quartz-apatite-REE phosphates-uraninite vein mineralization near Čučma (eastern Slovakia): A product of early Alpine hydrothermal activity in the Gemeric Superunit, Western Carpathians. *J. Geosci.* **2014**, *59*, 209–222. [[CrossRef](#)]
11. Ferenc, Š.; Rojkovič, I.; Mato, L. Uranyl minerals of Western Carpathians. In *Mineralogy of Bohemian Massif and Western Carpathians*; Conference Proceedings; Zimák, J., Ed.; Palacký University: Olomouc, Czech Republic, 2003; pp. 17–23. (In Slovak)
12. Ferenc, Š.; Biroň, A.; Sejkora, J.; Sýkorová, M. Phosphuranylite from the oxidation zone of the vein quartz-apatite-REE-U mineralization at Majerská Valley near Čučma (Slovenské Rudohorie Mts., Gemeric Unit). *Bull. Miner. Petrolog.* **2017**, *25*, 23–32. (In Slovak)
13. Ferenc, Š.; Mikuš, T.; Spišiak, J.; Milovská, S. Supergene minerals in quartz fluorapatite hydrothermal veins with U-Mo and U-REE mineralization near Čučma (Gemic Unit, Western Carpathians, eastern Slovakia): Preliminary study. In *Proceedings from Mineralogical-Petrological Conference Petros*; Ondrejka, M., Fridrichová, J., Eds.; FNS UK: Bratislava, Slovakia, 2019; pp. 17–19.
14. Mahel, M.; Vozár, J. Contribution to knowledge of Permian and Triassic in the North-Gemic syncline. *Geol. Pr. Spr.* **1971**, *56*, 47–66. (In Slovak)
15. Snopko, L.; Ivanička, J. Considerations on the paleogeography in the Lower Paleozoic of Spišsko-Gemerské Rudohorie Mts. In *Paleogeographical Evolution of the Western Carpathians*, 1st ed.; Vozár, J., Ed.; Geological Institution of D. Štúr: Bratislava, Slovakia, 1978; pp. 269–280. (In Slovak)
16. Ivanička, J.; Snopko, L.; Snopková, P.; Vozárová, A. Gelnica Group—Lower Unit of Spišsko-Gemerské Rudohorie Mts. (West Carpathians), Early Paleozoic. *Geol. Zbor. Geol. Carpath.* **1989**, *40*, 483–501.
17. Vozárová, A. Variscan metamorphism and crustal evolution of the Gemericum. *Západ Karpaty. Sér. Miner. Petrogr. Geochém. Metalogen.* **1993**, *16*, 55–117. (In Slovak)
18. Putiš, M.; Sergeev, S.; Ondrejka, M.; Larionov, A.; Siman, P.; Spišiak, J.; Uher, P.; Paderin, I. Cambrian–Ordovician metaigneous rocks associated with Cadomian fragments in the West-Carpathian basement dated by SHRIMP on zircons: A record the Gondwana active margin setting. *Geol. Carpath.* **2008**, *59*, 3–18.
19. Faryad, S.W. Metamorphism of the Early Paleozoic salic to intermediate volcanic rocks. *Miner. Slov.* **1991**, *23*, 325–332. (In Slovak)
20. Faryad, S.W. Metamorphism of the Early Paleozoic sedimentary rocks in Gemericum. *Miner. Slov.* **1991**, *23*, 315–324. (In Slovak)
21. Bajanič, Š.; Hanzel, V.; Mello, J.; Pristaš, J.; Reichwalder, P.; Snopko, L.; Vozár, J.; Vozárová, A. *Explanation to Geological Map of the Slovenské Rudohorie Mts.—Eastern Part, 1:50,000*, 1st ed.; State Geological Institute of D. Štúr: Bratislava, Slovakia, 1983; 223p. (In Slovak)
22. Bajanič, Š.; Ivanička, J.; Mello, J.; Reichwalder, P.; Pristaš, J.; Snopko, L.; Vozár, J.; Vozárová, A. *Geological Map of the Slovenské Rudohorie Mts.—Eastern Part, 1:50,000*, 1st ed.; State Geological Institute of D. Štúr: Bratislava, Slovakia, 1984. (In Slovak)
23. Uher, P.; Broska, I. Post-orogenic Permian granitic rocks in the Western Carpathian–Pannonian area: Geochemistry, mineralogy and evolution. *Geol. Carpath.* **1996**, *47*, 311–321.
24. Šefara, J.; Bielík, M.; Vozár, J.; Katona, M.; Szalaiová, V.; Vozárová, A.; Šimonová, B.; Pánisová, J.; Schmidt, S.; Götze, H.J. 3D density modelling of Gemeric granites of the Western Carpathians. *Geol. Carpath.* **2017**, *68*, 177–192. [[CrossRef](#)]
25. Vozárová, A.; Šarinová, K.; Sergeev, S.; Larionov, A.; Presnyakov, S. Late Cambrian/Ordovician magmatic arc type volcanism in the Southern Gemericum basement, Western Carpathians, Slovakia: U–Pb (SHRIMP) data from zircons. *Int. J. Earth Sci.* **2010**, *99*, 17–37. [[CrossRef](#)]
26. Vozárová, A.; Rodionov, N.; Šarinová, K.; Presnyakov, S. New zircon ages on the Cambrian–Ordovician volcanism of the Southern Gemericum basement (Western Carpathians, Slovakia): SHRIMP dating, geochemistry and provenance. *Int. J. Earth Sci.* **2017**, *106*, 2147–2170. [[CrossRef](#)]
27. Grecula, P.; Kobulský, J.; Gazdačko, L.; Németh, Z.; Hraško, L.; Novotný, L.; Maglay, J. *Geological Map of the Spišsko-Gemerské Rudohorie Mts., 1:50,000*, 1st ed.; State Geological Institute of D. Štúr: Bratislava, Slovakia, 1984. (In Slovak)
28. Grecula, P.; Kobulský, J.; Gazdačko, L.; Németh, Z.; Hraško, L.; Novotný, L.; Maglay, J.; Pramuka, S.; Radvanec, M.; Kucharič, L.; et al. *Explanations to Geological Map of the Spišsko-Gemerské Rudohorie Mts., 1:50,000*, 1st ed.; State Geological Institute of D. Štúr: Bratislava, Slovakia, 2011; p. 308. (In Slovak)
29. Montel, J.M.; Foret, S.; Veschambre, M.; Nicollet, C.; Provost, A. Electron microprobe dating of monazite. *Chem. Geol.* **1996**, *131*, 37–53. [[CrossRef](#)]

30. Pouchou, J.L.; Pichoir, F. "PAP" ( $\rho\rho Z$ ) procedure for improved quantitative microanalysis. In *Microbeam Analysis*; Armstrong, J.T., Ed.; San Francisco Press: San Francisco, CA, USA, 1985; pp. 104–106.
31. Makovicky, E.; Makovicky, M. Representation of composition in the bismuthinite–aikinite series. *Can. Miner.* **1978**, *16*, 405–409.
32. Zakrzewski, M.A.; Makovicky, E. Izoklakeite from Vena, Sweden, and the kobellite homologous series. *Can. Miner.* **1986**, *24*, 7–18.
33. Rojkovič, I.; Novotný, L. Uranium mineralization in Gemericum. *Miner. Slov.* **1993**, *25*, 368–370. (In Slovak)
34. Rojkovič, I. *Uranium Mineralization in Slovakia*, 1st ed.; Comenius University: Bratislava, Slovakia, 1997; p. 117.
35. Novotný, L.; Čížek, P. New occurrence of uranium and gold, southern from Prakovce in Spišsko-gemerské Rudohorie Mts. *Miner. Slov.* **1979**, *11*, 188–190. (In Slovak)
36. Rojkovič, I.; Háber, M.; Novotný, L. U–Au–Co–Bi–REE mineralization in the Gemeric Unit (Western Carpathians, Slovakia). *Geol. Carpath.* **1997**, *48*, 303–313.
37. Novotný, L.; Háber, M.; Križani, I.; Rojkovič, I.; Mihál, F. Gold in Early Paleozoic rocks in the central part of the Spišsko-gemerské rudohorie Mts. *Miner. Slov.* **1999**, *31*, 211–216. (In Slovak)
38. Rojkovič, I. U–Mo–Cu mineralization at Matejovce nad Hornádom. *Miner. Slov.* **1996**, *28*, 491–500. (In Slovak)
39. Nash, J.T. *Volcanic Uranium Deposits—Geology, Geochemical Processes, and Criteria for Resource Assessment*; Open-File Report; U.S. Geological Survey: Reston, VA, USA, 2010.
40. Breit, G.N.; Hall, S.M. *Deposit Model for Volcanogenic Uranium Deposits*; Open-File Report; U.S. Geological Survey: Reston, VA, USA, 2011.
41. Castor, S.B.; Henry, C.D. Geology, geochemistry, and origin of volcanic rock-hosted uranium deposits in northwestern Nevada and southeastern Oregon, USA. *Ore Geol. Rev.* **2000**, *16*, 1–40. [[CrossRef](#)]
42. Wilde, A.; Otto, A.; Jory, J.; MacRae, C.; Pownceby, M.; Wilson, N.; Torpy, A. Geology and mineralogy of uranium deposits from Mount Isa, Australia: Implications for albitite uranium deposit models. *Minerals* **2013**, *3*, 258–283. [[CrossRef](#)]
43. McKay, A.D.; Mieozitis, Y. *Australia's Uranium Resources, Geology and Development of Deposits*; AGSO-Geoscience: Canberra, Australia, 2001; pp. 1–184.
44. Dahlkamp, F.J. *Uranium Deposits of the World*; Springer: Berlin/Heidelberg, Germany, 2016; p. 792.
45. Rojkovič, I.; Puškelová, L.; Khun, M.; Medved, J. U–REE–Au in veins and black shales of the Gemericum, Slovakia. In *Mineral Deposits: From Their Origin to Their Environmental Impacts*; Conference Proceedings; Pašava, J., Kříbek, B., Žák, K., Eds.; Balkema: Rotterdam, The Netherlands, 1995; pp. 789–792.
46. Radvanec, M.; Konečný, P.; Ondrejka, M.; Putiš, M.; Uher, P.; Németh, Z. The Gemeric granites as an indicator of the crustal extension above the Late-Variscan subduction zone during the Early Alpine riftogenesis (Western Carpathians): An interpretation from the monazite and zircon ages dates by CHIME and SHRIMP methods. *Miner. Slov.* **2009**, *41*, 381–394. (In Slovak)
47. Broska, I.; Uher, P. Whole-rock chemistry and genetic typology of the West-Carpathian Variscan granites. *Geol. Carpath.* **2001**, *52*, 79–90.
48. Kubiš, M.; Broska, I. The role of boron and fluorine in evolved granitic rock systems (on the example of the Hnilec area, Western Carpathians). *Geol. Carpath.* **2005**, *56*, 193–204.
49. Kubiš, M.; Broska, I. The granite system near Betliar village (Gemic Superunit, Western Carpathians): Evolution of a composite silicic reservoir. *J. Geosci.* **2010**, *55*, 131–148. [[CrossRef](#)]
50. Broska, I.; Kubiš, M. Accessory minerals and evolution of tin-bearing S-type granites in the western segment of the Gemeric Unit (Western Carpathians). *Geol. Carpath.* **2018**, *59*, 483–497. [[CrossRef](#)]
51. Villaseñor, G.; Catlos, E.J.; Broska, I.; Kohút, M.; Hraško, L.; Aguilera, K.; Etzel, T.M.; Kyle, R.; Stockli, D.F. Evidence for widespread mid-Permian magmatic activity related to rifting following the Variscan orogeny (Western Carpathians). *Lithos* **2021**, *390–391*, 106083. [[CrossRef](#)]
52. Finger, F.; Broska, I. The Gemeric S-type granites in southeastern Slovakia: Late Palaeozoic or Alpine intrusions? Evidence from electron-microprobe dating of monazite. *Schweiz Miner. Petrogr. Mitt.* **1999**, *79*, 439–443.
53. Poller, U.; Uher, P.; Broska, I.; Plašienka, D.; Janák, M. First Permian—Early Triassic zircon ages for tin-bearing granites from the Gemeric unit (Western Carpathians, Slovakia): Connection to the post-collisional extension of the Variscan orogen and S-type granite magmatism. *Terra Nova* **2002**, *14*, 41–48. [[CrossRef](#)]
54. Kohút, M.; Stein, H. Re–Os molybdenite dating of granite-related Sn–W–Mo mineralisation at Hnilec, Gemeric Superunit, Slovakia. *Miner. Petrol.* **2005**, *85*, 117–129. [[CrossRef](#)]
55. Pecho, J.; Beňka, J.; Gargulák, M.; Václav, J. *Geological Research of Stibnite Deposits in the Betliar–Čučma–Volovec Area*; State Geological Institute of D. Štúr Archive: Bratislava, Slovakia, 1981. (In Slovak)
56. Cohen, K.M.; Finney, S.C.; Gibbard, P.L.; Fan, J.X. The ICS International Chronostratigraphic Chart. *Episodes* **2013**, *36*, 199–204. [[CrossRef](#)] [[PubMed](#)]
57. Grandstaff, D.E. A kinetic study of the dissolution of uraninite. *Econ. Geol.* **1976**, *71*, 1493–1506. [[CrossRef](#)]
58. Finch, R.J.; Ewing, R.C. The corrosion of uraninite under oxidizing conditions. *J. Nuclear Mater.* **1992**, *190*, 133–156. [[CrossRef](#)]
59. Kotzer, T.G.; Kyser, T.K. O, U, and Pb isotopic and chemical variations in uraninite: Implications for determining the temporal and fluid history of ancient terrains. *Am. Miner.* **1993**, *78*, 1262–1274.
60. Alexandre, P.; Kyser, T.K. Effects of cationic substitutions and alteration in uraninite, and implications for the dating of uranium deposits. *Can. Miner.* **2005**, *43*, 1005–1017. [[CrossRef](#)]

61. Timón-Sánchez, S.M.; López-Moro, F.J.; Romer Elrhede, D.; Fernández-Fernández, A.; Moro-Benito, C. Late-Variscan multistage hydrothermal processes unveiled by chemical ages coupled with compositional and textural uraninite variations in W-Au deposits in the western Spanish Central System Batolith. *Geol. Acta* **2019**, *17.1*, 1–19.
62. Yuan, F.; Jiang, S.Y.; Liu, J.; Zhang, S.; Xiao, Z.; Liu, G.; Hu, X. Geochronology and geochemistry of uraninite and coffinite: Insights into ore forming process in the pegmatite-hosted uraniferous province, North Qinling, Central China. *Minerals* **2019**, *9*, 552. [[CrossRef](#)]
63. Corcoran, L.; Simonetti, A. Geochronology of uraninite revisited. *Minerals* **2020**, *10*, 205. [[CrossRef](#)]
64. Ruzicka, V. Vein uranium deposits. *Ore Geol. Rev.* **1993**, *8*, 247–276. [[CrossRef](#)]
65. Robinson, P.C. A genetic classification of Canadian uranium deposits. *Can. Miner.* **1958**, *6*, 513–521.
66. Lang, A.H.; Griffith, J.W.; Steacy, H.R. *Canadian Deposits of Uranium and Thorium*; Geological Survey of Canada: Ottawa, ON, Canada, 1962; p. 324.
67. Ruzicka, V. Geological comparison between East European and Canadian uranium deposits. *Geol. Surv. Can. Pap.* **1971**, *48–70*, 1–195.
68. Rich, R.A.; Holland, H.D.; Petersen, U. *Hydrothermal Uranium Deposits*; Elsevier: Amsterdam, The Netherlands, 1977; p. 264.